# Part I

# Fundamentals

# Chapter 2

# Formation and Analysis of Microbubbles

## 2.1 General

**Hideki Tsuge**
*Keio University, Tokyo 166-0004, Japan*
htsuge@jcom.home.ne.jp

### 2.1.1 Introduction

The formation methods of microbubbles (MBs) are divided into two cases: one is the gas is accompanied with liquid introduced and another is blowing the gas in quiescent liquid. In this chapter, MB formation methods and measuring methods of MB diameter are discussed. In the following sections, the formation methods by several makers and measuring methods of MB diameter and ζ potential are shown.

#### 2.1.1.1 With liquid flow

##### *2.1.1.1.1 Rotational liquid flow method*

Ohnari developed MB generator (M2-LM type, produced by Nanoplanet Research Institute Corp.) as shown in Fig. 2.1, which is cylindrical type (diameter 50 mm, height 100 mm) pressurized water is fed from the bottom water pipe by pump and rotational

*Micro- and Nanobubbles: Fundamentals and Applications*
Edited by Hideki Tsuge

ISBN 978-981-4463-10-2 (Hardcover), 978-981-4463-11-9 (eBook)
www.panstanford.com

liquid flow is produced in the cylinder [1]. By Bernoulli's theorem, the central part of the cylinder becomes low pressure produced by rotational liquid flow, and air is sucked automatically. Air swirling flow is formed, and MBs are produced near the outlet of cylinder. Liquid flow rate is about 12 L/min, and the swirling speed of two-phase flow in the cylinder is 300–600 round/s. The ratio of gas flow rate/liquid flow rate is 1/7–1/15. M2-LM type generator was used for the aquaculture of oysters in Hiroshima, and good growth promotion was reported by TV news.

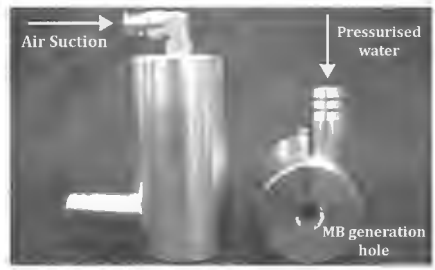


**Figure 2.1** Rotational liquid flow MB generator (M2-LM).

MB size distribution by M2-LM type generator is 10–50 μm, and the mode size is 15 μm. The concentration of MB by M2-LM is thinner than that by dissolved air flotation method. Li and Tsuge examined the following MB generating method [2]. The combination of the centrifugal pump (Nikuni Co. Ltd.) and the rotating-flow MB generator (M2-M, Nanoplanet Research Institute Corp.) was used. Water and air are sucked simultaneously by the pump. Some air dissolves into water before transporting to the generator. The pressurised water is then decompressed through the MB generator with a high rotating velocity.

Recently the inside of generator is divided by the partition, and the high-quality MB generator is produced by Aqua Air Co. [3].

#### *2.1.1.1.2 Static mixer type*

As shown in Fig. 2.2, static mixer (OHR Fluid Engineering Institute Corp.) induces helically two-phase flow by guide vane and mushroom-type projections (current cutter) and destructs to MB water (MB size 5–50 μm) whose production is maximum 1500 L/min [4].

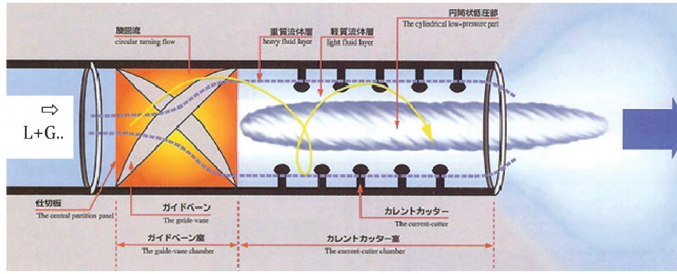


**Figure 2.2** Schematic diagram of OHR static mixer.

#### *2.1.1.1.3 Ejector type*

Ejector-type nozzle ejects liquid in high speed as aspirator, and gas is absorbed by the back pressure at the outlet, finally produces MBs by turbulent mixing and shearing mechanism. The average MB size produced is 424 μm [5].

#### *2.1.1.1.4 Venturi type*

When gas and liquid are simultaneously flowed in the squeezing part of Venturi tube, the sudden change of liquid flow rate produces shock wave and large bubbles are destroyed to MBs. To avoid bubble coalescence, 50 ppm 3-pentanol is added, in which case 100 μm MBs are mainly produced [6].

#### *2.1.1.1.5 Dissolved air floatation type*

Dissolved air floatation MB generator is shown in Fig. 2.3. About 3–4 atm pressurized air is dissolved into water and is flushed through the nozzle; the supersaturated air produces MBs in the water. The concentration of MBs is high, and the liquid is like milk. MB size distribution has two peaks as shown in Fig. 2.4.

### 2.1.1.2 Without liquid flow

#### *2.1.1.2.1 Capillary type*

Kukizaki sintered porous glass made of loamy soil and the nanobubbles (NBs) whose bubble diameter is 720 nm are formed from the sintered membrane of average pore size 84 nm [7]. To avoid the bubble coalescence, surface active agent is often added.

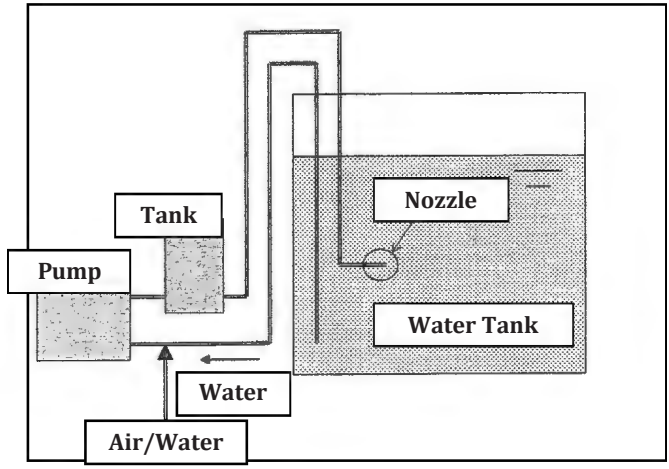


**Figure 2.3** Schematic diagram of dissolved air floatation MB generator.

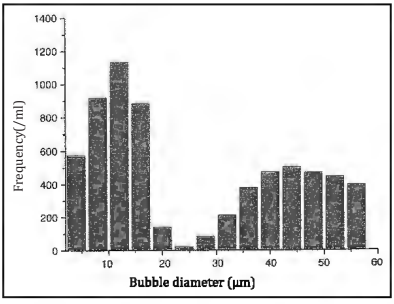


**Figure 2.4** Bubble size distribution of dissolved air floatation MB generator.

#### *2.1.1.2.2 Rotating type*

The rotor made of sintered material is rotated at high speed in the surrounding stator, and gas is automatically absorbed. Average 50 μm MBs are formed, and the reaction crystallization was conducted by Onoe et al. [8]. The merit of the generator is no need of liquid pump. The rotating-type generators are produced by Fuki Works Co., Nomura Electronics Co. and Royal Electric Co. and have been used for the purification of lakes and marshes.

#### *2.1.1.2.3 Ultrasound type*

Makuta et al. radiated ultrasound to the bubbles formed from the needle and produced same size MB (about 10 μm) in high viscosity liquid (100 cP) such as silicon oil [9]. This method is applicable for the production of homogeneous MBs and is proposed for the application of medical materials.

#### *2.1.1.2.4 Vapour condensation type*

When the mixed vapours of nitrogen and steam are blowing from nozzle into water, the steam condensates and non-condensable nitrogen MBs obtained. The mode diameter of MBs is 20–40 μm. MB size is affected by gas composition, nozzle diameter and vapour flow rate [10].

#### *2.1.1.2.5 Electrolysis type*

Tsuge et al. made electrolysis of water and found the effect of vibration of low frequency vibrating plates and electrolyte [11]. Average MB size is 35–55 μm, and its size distribution is 15–100 μm.

### 2.1.1.3 Measuring method of MB size

The measurement methods of MB are outlined in this section, and the details are shown in the following chapters.

#### *2.1.1.3.1 Visualization method*

Digital microscope and CCD (Charged Coupled Device) camera are used for the photograph of MBs, and processes graphically and MB sizes are measured. MBs less than 40 μm need microscope. Measurable MB size is larger than several μm.

#### *2.1.1.3.2 Laser diffraction/scattering method*

By radiation of laser beam, the diffraction scattering light of small bubbles scatters forward, backward and cross direction [12]. Such scattering pattern was measured, and by comparing the scattering pattern obtained by Mi scattering theory, the MB size distribution is obtained. MB size distribution between 10 nm and several mm is measurable.

#### *2.1.1.3.3 Coulter counter method*

When the electrodes are inserted in electrolyte solution surrounded by the partition wall having small hole and voltage is applied, the electrical resistance is controlled by the resistance in the small hole [13]. When the MBs pass through the hole, the electrical resistance increases so that the number and size of MB can be measured. The measurable range is 0.2–600 μm, whereas for more wide size ranges hole diameter should be changed.

#### *2.1.1.3.4 Dynamic light scattering method*

It is used for the measurement of NBs [3]. By Brownian motion, the observed NBs are diffusing and the laser light strength fluctuates. As the diffusivity of bubbles depends on bubble size, the bubble size is expressed by the fluctuation factor of laser light. By autocorrelation of fluctuation of scattering light, size distribution is obtained. As the exclusion of dust is necessary in measurement of NBs, membrane filter is used. To distinguish dust and NB, further check is necessary.

## References

1. Ohnari H (2006) *All on Microbubbles* (Nippon Jitsugyo Shuppan Co., Japan) (in Japanese).
2. Li P, Tsuge H (2006) Water treatment by induced air floatation using microbubbles, *J Chem Eng Japan,* **39**, 896–903.
3. Takahashi M (2009) Fundamentals and engineering applications of microbubbles and nanobubbles, *Material Integration,* **22**, 2–19 (in Japanese).
4. Uematsu H (2006) Advantage and Possibility of OHR Microbubble, *J. Resources and Environment,* **42**, 100–103 (in Japanese).
5. Nakatake Y, Watanabe K, Eguchi T (2007) Combustion improvement for diesel engines with ejector-type micro-bubble mixed fuel, *Trans Japan Soc Mechanical Eng,* **73**, 2368–2374 (in Japanese).
6. Fujiwara A (2006) Generating method of microbubbles by Venturi tube, *Eco Industry,* **22**, 27–30 (in Japanese).
7. Kukizaki M, Nakajima T, So G, Obama Y (2004) Formation and control of size of uniformly dispersed nanobubbles from porous glass membrane, *Kagaku Kogaku Ronbunshu*, **30**, 654–659 (in Japanese).

8. Onoe K, Matsumoto M, Akiya T (2002) Reactive crystallization of calcium carbonate using $CO_2$ micro-bubbles, *Bull Soc Sea Water Sci Japan,* **56**, 357–361 (in Japanese).
9. Makuta T, Takemura F, Hirahara E, Matsumoto Y, Shoji M (2004) Generation of micro gas bubbles of uniform diameter in an ultrasonic field, *Trans Japan Soc Mechanical Eng.*, **70**, 2758–2767 (in Japanese).
10. Terasaka K, Saito J, Toda Y, Kobayashi D (2009) Microbubble generation using direct-contact condensation of mixed vapor, *Progress in Multiphase Flow Research,* **4**, 103–110 (in Japanese).
11. Tsuge H, Ogawa T, Ohmasa R (2008) Microbubble formation by electrolysis using a new mixing equipment with low frequency vibratory fins, *J Chem Eng Japan,* **41**, 557–561.
12. Maruyama M (2007) *Laser Diffraction · Scattering Method,* The Latest Technology of Microbubbles and Nanobubbles CMC Book Co. Japan, pp. 31–41 (in Japanese).
13. Fujiwara A (2007) *Electrical Resistance Method,* The Latest Technology of Microbubbles and Nanobubbles CMC Book Co. Japan, pp. 42–45 (in Japanese).

## 2.2 New Type of Microbubble Generator by Two-Phase Flow Method

**Osamu Matsumoto**
*Aqua Air corporation, Tokyo Japan*
officematsumoto@apricot.ocn.ne.jp

### 2.2.1 Development Concept

The fundamental concept of this development was to make a useful microbubble generator in a wide variety of practical fields. Many kinds of generators were developed at the time, but most of them were too small for the practical usages. Considering the usages, the generator must be stable and reliable for generating microbubbles in the variety of practical sites for the operations of such as waste water treatment and environmental remediation.

The technical properties of the new developed device are as follows: easy on-site installation due to the simple structure, short setting time and effective operation with little consumption

electricity. Also, it is a very important point to predict the practical effect at the operation sites from the results of laboratory tests that the devices must demonstrate the same performance regardless of their size.

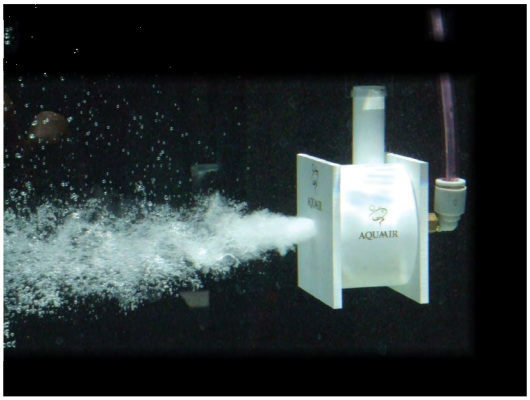


**Photo 2.1** Generation of millimetre bubbles.

The microbubble generator can produce any size of bubbles, from nanobubble to microbubble, according to the purposes, and we can offer the devices of various sizes according to your offer.

### 2.2.2 Method of Bubble Generation

Our microbubble generator is classified to the two-phase (gas and water) turbulent type, and the generator uses ultra-high-speed turning flow method by multiple cylinder structure.

### 2.2.3 Structural Feature

The ultra-high-speed swirl flow along the centre line of the device is the most important operation for the stable generation of a large amount of tiny bubbles, and this is a patented work (Japan Patent No. 3890076).

As shown in Photo. 2.1, the water is introduced into the apparatus by a pump, and the circulating rate of the water flow is accelerated as the water is going through the multiple cylinders from the outer to the centre one. A gas was automatically introduced from the gas

inlet owing to the pressure drop caused by circulating flow, and a tornado-like twirl of gas formed along the centre axis was forced out from the outlet with circulating water. The mixture of gas and water was dispersed by the force of circulation, and the shearing force generated at the outlet separated the mixture into fine bubbles.

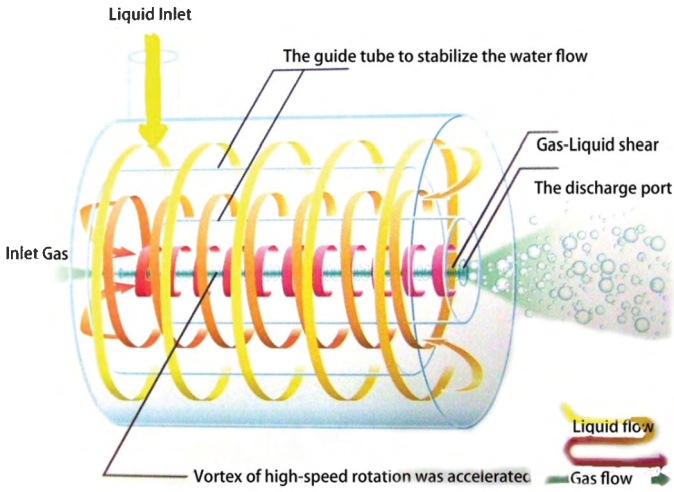


**Figure 2.5** Schematic diagram of the generator.

It is a superior point of this apparatus to generate a large amount of fine bubbles through a hydrodynamic mechanism characterised by the control of ultra-fast twirling speed.

The schematic diagram of the microbubble generator is shown in Fig. 2.5. The apparatus have been designed to accelerate the circulating flow in the cylindrical body, and the interior region is separated by two built-in cylinders with different radii. The circulating speed is increasing and, in the case of our $\phi$45 mm bubble generator, the speed finally reaches about 1000 rpm at the outlet according to the evaluation by an ultra-high speed camera.

### 2.2.4 Characteristics of the Microbubble Generator

- The typical multiple cylinder structure of the generator enables the apparatus to generate a fair amount of microbubbles, and the stable operation of the internal swirling vortex flow

controlled by the built-in cylinders permits the usages at a wide variety of sites from a small laboratory scale to a large industrial and environmental scale.

- Since there are no moving parts with very simple structure, there is no mechanical trouble; users can choose the generators of various materials, such as plastics, ceramic and stainless steel, depending on the applications.
- Excellent operating efficiency of the apparatus, which works only for the injection pump.
- By adjusting the amount of injecting gas volume, the bubbles changes their diameter from millimetre scale to nanometre scale dimension.
- Not only the liquid–gas combination but also the liquid–liquid combination is also available. So the apparatus can be used to generate fine emulsification, dispersion, fine mist and fine bubbles.
- Gas or liquid as an inhalation medium is automatically taken into the apparatus through the gas inlet caused by the pressure drop due to the high-speed circulation of water flow.

### 2.2.5 Appearances of the Generator: Shape and Dimensions

The apparatus is available in various sizes from ϕ10 mm to bigger than ϕ600 mm.

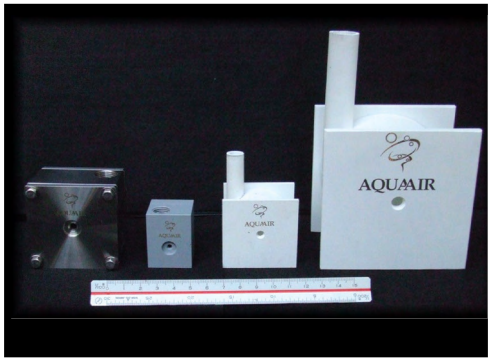


**Photo 2.2** Microbubble generator ϕ20 mm–ϕ90 mm.

**Photo 2.3** Microbubble generator ϕ300 mm for shrimp ponds.

### 2.2.6 Operating Status of the Bubble Generator

**Photo 2.4** Microbubble generator ϕ45 (standard type) in operation.

**Photo 2.5** Function test of ϕ300 at laboratory.

**Photo 2.6** Operation of Microbubble generator ϕ300 at a shrimp ponds.

## 2.2.7 Practical Applications of the Microbubble Generators

### 2.2.7.1 Big-sized bubble generator

**Photo 2.7** Photograph of the pond before the installation of microbubble generator.

1. Installation of a microbubble generator at a shrimp pond (2.5 m water depth 100 m × 100 m): Microbubble generator ϕ300 was installed in the pump and operated from the beginning of October to the end of November. It was a little bit late to examine the direct effect on microbubble on the

growth of shrimp, but we recognised the effect on the colour of water suggesting a good condition for plankton in the pond owing to the enough oxygen supply.
2. It is expected to use the generators for the improvement of water quality at lakes, source of drinking water, by the environmental remediation due to oxygen supply to bottom.

#### 2.2.7.2 Medium-sized bubble generator

1. As shown in the pictures below, medium-type generators were used to activate shrimps for marketing in a water reservoir (1 m depth 15 m × 1 m). Fairly good results were obtained for maintaining the freshness of shrimps.
2. It is expected to be used as a new type of cleaning in position. Tests were conducted at plants for food and cosmetic and succeeded to reduce the amount of chemicals and the operating temperature.
3. Ozone microbubble is expected for wastewater treatments.
4. You can use the generators to produce emulsion very effectively by introducing liquid instead of gas through the gas inlet. The emulsion produced by the generator is stable because of the surface electricity of suspended emulsions.

**Photo 2.8** Medium-sized bubble generation device status (ϕ75) set.

**Photo 2.9** Medium-sized bubble generation device operating conditions ($\phi$75).

#### 2.2.7.3 Small-sized bubble generation equipment

1. This type of generator is very useful for laboratory tests because of low electricity consumption.
2. The generator is small enough to be embedded into consumer products and operates efficiently as eco-products in future.
3. We are planning to manufacture a much smaller generator to be used at a variety of technical fields.

We are now conducting several kinds of tests for the future applications such as surface cleaning and wastewater treatment by using variety of gases including ozone and carbon dioxide. Since the apparatus can be used to generate emulsion, we are also conducting experiments regarding the mixing efficiency and the stabilisation of fine emulsions. Most of these tests are carried out according to the agreements of confidentiality with many private companies.

### 2.2.8 Measurement of Size Distribution of Microbubbles

The size distributions of microbubbles generated by the generators were evaluated by a liquid particle counter at National Institute of Advanced Industrial Science and Technology.

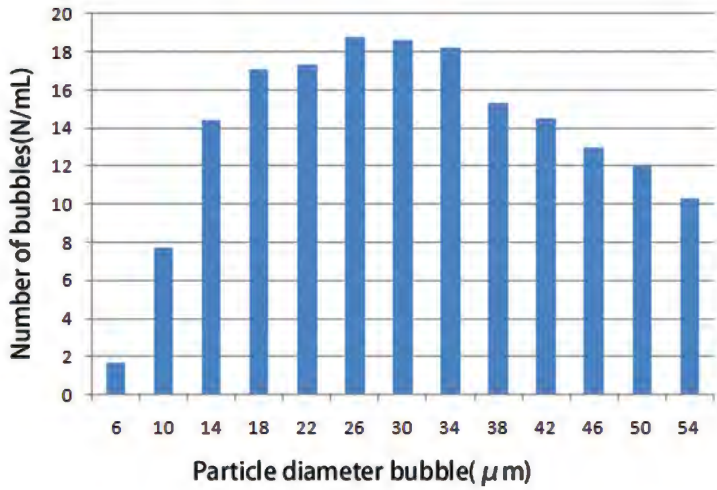


**Figure 2.6** Size distribution of microbubbles generated by the generator of ϕ10 mm (Shower-head type) in tap water. This generator is very small but can produce a lot of microbubbles constantly.

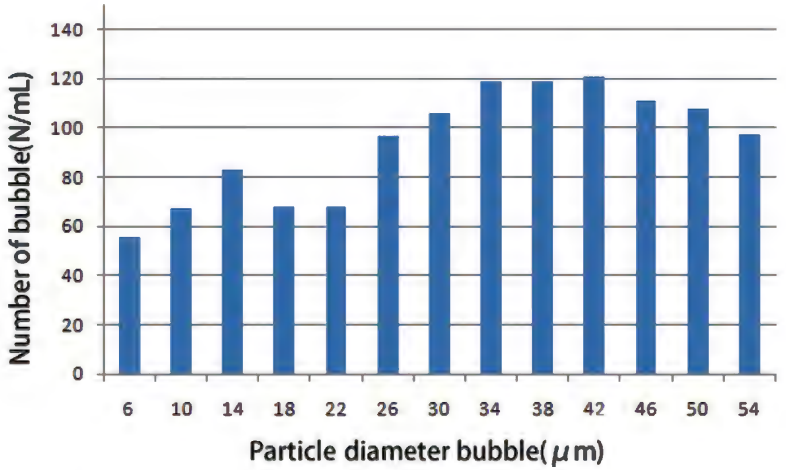


**Figure 2.7** Size distribution of microbubbles generated by the generator of ϕ40 mm in seawater. The generators can produce a fairly high concentration of microbubbles because of the effects of electrolytes in seawater. It has been recognised that there are two peaks in the size distribution in seawater.

### 2.2.9 Experimental Study for Shrimp Farming Technology

We have been conducting the experimental study for shrimp farming using the microbubble technology for the future applications. Laboratory cultivation was carried out, and it has been demonstrated that the survival rate would be doubled compared with the conventional methods. We hope to contribute to make the sustainable society all over the world by using our microbubble technology.

## 2.3 Measurement and Analysis

### 2.3.1 Simulation of Microbubble Coalescence and Repulsion

**Tomoaki Kunugi[a] and Yukihiro Yonemoto[b]**
[a]*Department of Nuclear Engineering, Kyoto University, Yoshida, Sakyo, Kyoto 606-8501, Japan*
[b]*Priority Organization for Innovation and Excellence, Kumamoto University, Kumamoto-shi, Kumamoto, Japan*
kunugi@nucleng.kyoto-u.ac.jp, yonemoto@mech.kumamoto-u.ac.jp

The mechanism of bubble coalescence/repulsion is still unclear, and this problem of bubble coalescence/repulsion is a key issue when it comes to numerical research on multiphase flows. Experimental studies have revealed that not only the concentration of the electrolyte dissolved in water but also the existence of ion pairs plays an important role in bubble coalescence. However, no appropriate numerical models have been developed until now. The bubble coalescence mechanism may be related to thermodynamics, electromagnetics, hydrodynamics, heat and mass transfer and so on. In this chapter, microbubble interaction on the basis of a new gas–liquid interfacial model with the coalescence model is discussed, and the mass transfer is also considered in the numerical simulation. The results indicated that the contamination at the interface had an important effect on microbubble coalescence and repulsion.

### 2.3.1.1 Introduction

On a macroscopic scale corresponding to bulk fluid flows, a gas–liquid interface has been characterised by discontinuous physical properties, such as density, viscosity and so on. On the other hand, on a microscopic scale corresponding to molecular motion, the physical properties at the interface continuously vary from the gas phase to the liquid phase. This implies that interfacial phenomena can be characterised by various time and space scales. Therefore, the modelling of the gas–liquid interface, whose physical properties vary during transition from micro- to macroscopic scale, has been known as a big problem in multiphase flow science and engineering. Especially, the mechanism of bubble coalescence/repulsion has not yet been clarified. At the gas–liquid interface, many complicated phenomena, such as evaporation, condensation, electrokinetics, and heat and mass transfer, occur. Interfacial interactions such as bubble coalescence/repulsion may be affected by these interfacial phenomena.

Experimental research on bubble coalescence/repulsion mainly focuses on the effects of the concentration of the electrolyte on the behaviour and coalescence threshold of the bubbles in the liquid [1–3]. These researches revealed that the ions adsorbed at the gas–liquid interface, the combination of these ions and electrolyte concentration were important factors in bubble coalescence/repulsion. Contamination at the interface could greatly influence bubble coalescence/repulsion because these contaminations might be related to the heat and mass transfer and electrochemistry around the interface [4,5]. A coalescence model for a combination of simple ions has been theoretically proposed [6]. It focused on determining the impact of repulsive interaction based on the results from the formation of an electric double layer around the interface on bubble coalescence. However, a detailed mechanism has not yet been elucidated.

On the other hand, in theoretical and numerical studies, interfacial interactions were considered on the basis of hydrodynamic lubrication theories [7,8]. In such lubrication theories, bubble coalescence was modelled based on a drainage mechanism, where the liquid existing between two bubbles drained from the liquid film. This theory was based on the premise of the existence of a liquid film. Recently, the contamination at the interface has been considered in the lubrication theory, and the

Marangoni effect on the drainage mechanism has been discussed [9]. Contaminants such as adsorbed materials or ions at the interface were strongly related to heat and mass transfer of the liquid, and they might affect the timing of bubble coalescence [9,10]. Moreover, the interfacial interaction of bubbles in fluid flow would be also affected by the fluid vortical motion around the bubbles. However, in the research on the interfacial interactions based on the lubrication theories, the formation mechanism of the liquid thin film has not been discussed yet. Thus, there are still problems remaining with respect to the clarification of the mechanism of bubble coalescence/repulsion.

Because of the background mentioned above, focusing on the effect of an electrostatic potential due to contamination at the interface on the microbubble interaction, we have been conducted the numerical simulation of the microbubble interaction. In this chapter, some numerical results of microbubble coalescence/repulsion process are shown, and the phenomenon is discussed.

#### 2.3.1.2 Electrostatic effect on microbubble interaction and mass transfer

In our previous study [11], the numerical simulation of bubble interaction was conducted by considering an interaction force as a kind of a Coulomb force. With respect to the bubble interaction in the numerical simulation, a distance between the centres of two bubbles was calculated using a labelling method, which was a popular manner in the image analyses. It was modelled that the interaction force acts on the bubble surface cells when the distance between two bubble centres became smaller than a certain distance. Then, the bubble velocity after the interaction was calculated by satisfying the momentum and kinetic energy conservations. The calculated velocity was set on the numerical cells of bubble surface. Figure 2.8 depicts a numerical simulation result of the microbubble interaction: the diameter of the microbubble was 100 m, and the comparison of numerical results to the experimental observation. In the numerical result, as shown in Fig. 2.8, one bubble is sliding downwards along the surface of the other bubble. It is found that the numerical result retrieves the bubble behaviour well compared with the experimental observation. This result indicated the importance of an interfacial electrostatic potential in the microbubble interaction. To model the microbubble

coalescence and repulsion physically in the numerical simulation, the electric effect of ions and contamination adsorbed at the surface on the bubble interaction must be considered from the thermodynamic point of view. Moreover, the contamination surrounding the bubbles in fluid such as mass transfer cannot be ignored.

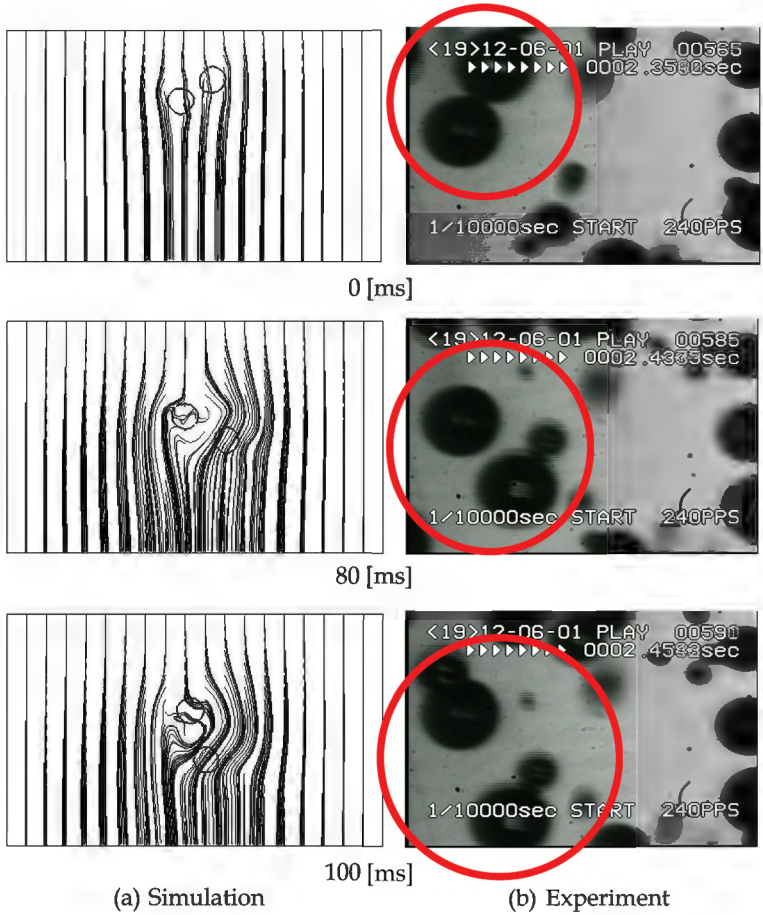


**Figure 2.8** Interaction of microbubbles.

Thus, in order to elucidate the mechanism of bubble coalescence and repulsion, we have developed a new thermodynamic and mathematical interfacial model on the basis of the phase field theory [12] associated with the multiscale concept ranging from micro- to

macroscopic scales in order to consider the multiscale physics at the interface. In this modelling, the interface was assumed to be a finite thickness like a thin liquid membrane, and the free energy including the electric charge due to a contamination was derived at the microscopic scale, that is the interface thickness. The free energy was incorporated into the Navier–Stokes equation as source terms based on the Chapman–Enskog expansion [13]. Finally, the multiscale multiphase flow equation was derived [14]. On the other hand, at the macroscopic point of view, the interfacial jump condition based on thermodynamics was also derived using the multiscale multiphase flow equation [15]. In that work, the jump condition at the interface was mainly characterised by the curvature related to the shape of the interface, which means that the interface is a mathematical surface: it means zero thickness. Therefore, the jump condition is considered as a macroscopic interfacial equation. Especially, a theoretical consideration of the interfacial interaction on the basis of the thermodynamic interfacial jump condition [16] indicated that the electrostatic force caused by the contamination adsorbed at the interface distorted the shape of bubble surface and formed a liquid thin film between interfaces.

#### 2.3.1.3 Modelling and simulation of microbubble coalescence and repulsion

Many pieces of experimental evidence revealed the importance of the electrolytes and the adsorbed ions at the interface with respect to bubble coalescence [1–3]. This indicates that the mass transfer cannot be ignored to consider interfacial interactions. According to the Henry's law, the amount of a gas dissolved in a liquid is proportional to the gas pressure at the bubble surface in equilibrium when the system is at a constant temperature. It is very difficult to make the perfectly purified water in which there is no contamination. Thus, a relationship between the dissolved gas and the contamination in the liquid would be very important in the interfacial interaction. In our study, the coalescence model of microbubbles has been developed by applying a conventional nucleation theory [17] combined with the concept of the contamination in the liquid regarding to the mass transfer considered between the interfaces. The numerical results of microbubble interactions on the basis of the multiscale multiphase

flow equation, and the coalescence model [18,19] are discussed in the following sections.

Figure 2.9 depicts the results of microbubble interactions obtained by two-dimensional numerical simulation. In the simulation, the coalescence model and the electrostatic potential at the interface were considered. In case 1, both the electrostatic potential at the interface and the coalescence model were not considered. In case 2, both models were considered. In case 1, the microbubbles at 1.50 ms were just contacted before the coalescence. Then, two microbubbles coalesced with each other at 2.00 ms. On the other hand, in case 2, the microbubbles maintained a constant distance at 1.50 ms. After that, two microbubbles coalesced with each other at 2.25 ms. Obviously, the timing of coalescence in case 2 delayed from case 1. This behaviour was also observed in our experiment [10].

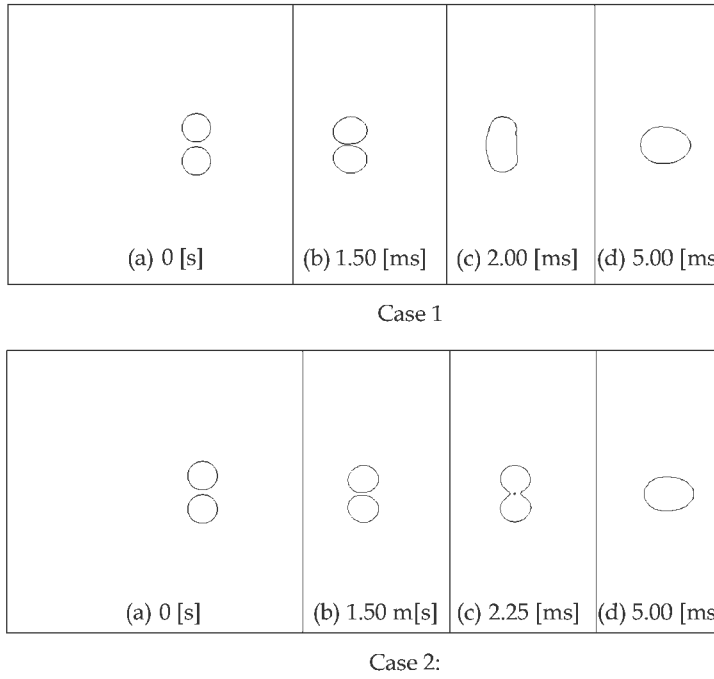


**Figure 2.9** Numerical results of microbubble coalescence (cases 1 and 2: electrostatic potential 0 (V) and $-1.0 \times 10^{-5}$ (V), electric conductivity 103.146 (S/cm)).

In the three-dimensional numerical simulation, similar results were obtained in a simulation where the model of the interfacial electrostatic potential was only considered. Especially, the thin liquid film was observed between two microbubble interfaces as shown in Fig. 2.10a. This result reveals that the pressure in the liquid film is lower than the bulk pressure around the microbubbles as shown in Fig. 2.10b. This means that the bulk liquid flows into the thin liquid film to satisfy the continuity and maintain a certain thickness of the liquid film. Eventually, the general drainage explanation based on the lubrication theory [7], which is based only on hydrodynamics, cannot explain the premise of the existence of a liquid film between two microbubbles. Therefore, the present numerical results could prove that the contamination at the interface (electrostatic potential) is very important with respect to the bubble interaction.

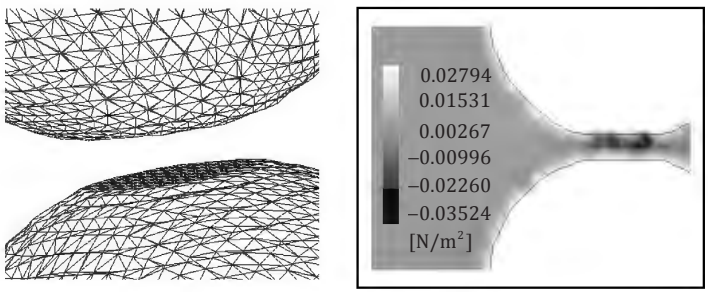


**Figure 2.10** Microbubble interaction in three-dimensional simulation. (a) Liquid film in three dimensions. (b) Pressure distribution in liquid film.

### 2.3.1.4 Summary

The present numerical results indicate the possibility that bubble interactions on the mesoscopic scale can be simulated by using the multiscale multiphase flow equation. At the present, our interfacial model does not perfectly consider the various physical phenomena occurring at the interface. Thus, there may be some processes with respect to bubble coalescence in addition to those considered in the present coalescence model. However, at least, it can be seen that there are two coalescence processes: one process is related to only the electrostatic potential, and the other is related to mass transfer in addition to the electrostatic potential. In order to understand

the mechanism of microbubble coalescence, the theoretical and experimental investigations of the phenomena should be continued.

## References


1. Craig VSJ (2004) Bubble coalescence and specific-ion effects, *Curr Opin Colloid Interface Sci,* **9**, 178.
2. Henry CL, Craig VSJ (2008) Ion-specific influence of electrolytes on bubble coalescence in nonaqueous solvents, *Langmuir,* **24**, 7979.
3. Marčelja S (2004) Short-range forces in surface and bubble interaction, *Curr Opin Colloid Interface Sci,* **9**, 165.
4. Joshi KS, Braumann A, Jeelani SAK, Blickenstorfer C, Naegeli I, Windhab EJ (2009) Mechanism of bubble coalescence induced by surfactant covered antifoam particles, *J Colloid Interface Sci,* **339**, 446.
5. Auster ND, Gunde R, Mäder R, Windhab EJ (2009) Binary coalescence of gas bubbles in the presence of a non-ionic surfactant, *J Colloid Interface Sci,* **333**, 579.
6. Marčelja S (2006) Selective coalescence of bubbles in simple electrolytes, *J Phys Chem* B, **110**, 13062.
7. Reynolds O (1886) On the theory of lubrication and its application to Mr. Beauchamp Tower's experiments, including an experimental determination of the viscosity of olive oil, *Philos Trans R Soc Lond,* **177**, 157.
8. Kaur S, Leal LG (2009) Three-dimensional stability of a thin film between two approaching drops, *Phys Fluids,* **21**, 072101.
9. Leshansky AM (2001) On the influence of mass transfer on coalescence of bubbles, *Int J Multiphase Flow,* **27**, 189.
10. Yonemoto Y, Yanagisawa H, Kawara Z, Kunugi T (2008) Coalescence of microbubble, *J JSEM*, **8**(1), 38–44, ISSN 13464930.
11. Matsumoto Y, Fukami T, Kunugi T, Serizawa A (2001) Fluid-dynamic structure of air-water bubbly flow with micro-bubbles, in *Proceedings of the 4th International Conference on Multiphase Flow*, New Orleans LA, USA, CDROM_332.
12. Cahn JW, Hilliard JE (1958) Free energy of a nonuniform system. I. Interfacial energy, *J Chem Phys,* **28**(2), 258–267.
13. Chapman S, Cowling T (1970) *The Mathematical Theory of Non-uniform Gases,* 3rd ed, Cambridge University Press, Cambridge.
14. Yonemoto Y, Kunugi T (2010) Multi-scale modeling of the gas-liquid interface based on mathematical and thermodynamic approaches, *Open Transport Phenom J*, **2**, 69–79.

15. Yonemoto Y, Kunugi T (2011) Macroscopic gas-liquid interfacial equation on the basis of thermodynamics and mathematical approaches, in *Mass Transfer—Advanced Aspects* (Hironori N ed), InTech, Rijeka, Croatia.
16. Yonemoto Y, Kunugi T (2008) Analytical consideration of thermodynamic jump condition, *Progress in Multiphase Flow Research*, **3**, 27–34 (in Japanese).
17. Abraham FF (1974) *Homogeneous Nucleation Theory,* Academic Press, NY, USA.
18. Yonemoto Y, Kunugi T (2010) Fundamental numerical simulation of microbubble interaction using multi-scale multiphase flow equation, *Microgravity Sci Technol*, **22**, 397–405.
19. Yonemoto Y, Kunugi T (2009) Fundamental study of microbubble coalescences based on multi-scale multiphase flow equations, *Trans JSME Ser B*, **75**, 1790–1797 (in Japanese).

## 2.3.2 Physical Property Evaluation by $\zeta$-Potential

**Yuka Yoshida, Norihito Kawaguchi, and Nobuhiko Kubota**
*Advanced Applied Science Department, Research Laboratory, IHI Corporation, Yokohama 235-8501, Japan*
yuka_yoshida@ihi.co.jp

### 2.3.2.1 Introduction

Application of various technologies using microbubbles is expected. In these days, some medical treatments and industry applications have already started. However, when the microbubbles are applied, many unknown physical properties, for example, the electrification state of the surface of the microbubbles and a collapse phenomenon, are still left.

In this study, it is investigated to elucidate the electrification state of the surface of the microbubbles by measuring the $\zeta$-potential of the microbubbles.

The $\zeta$-potential of the microbubbles is reported by Takahashi [1]. He measured the $\zeta$-potential of air microbubbles and obtained the results that the $\zeta$-potential of air microbubbles does not depend on the size of the microbubbles and depends on the changing of pH of a solvent. Then, in order to investigate the properties of the microbubbles other than of the air, the $\zeta$-potential measurement of the microbubbles of argon gas was

tried. Moreover, the ζ-potential measurement of air microbubbles was also tried for comparison with Takahashi's measurement result.

### 2.3.2.2 Experiment

#### *2.3.2.2.1 Measuring method and conditions of ζ-potential*

The ζ-potential was measured with air and argon microbubbles. Microbubble generator (4-MDG-045, Aura Tech) was used for creation of the microbubbles. Ion-exchanged water was used as a solvent, and water temperature was set to 25 ± 5°C. Chloride was used for adjustment of pH, and it was set to pH 3. The equipment is shown in Fig. 2.11 using microscopic electrophoresis as the measuring method of the ζ-potential of the microbubbles [2]. The voltage of 20 V/cm was applied to the observation cell of the microbubbles.

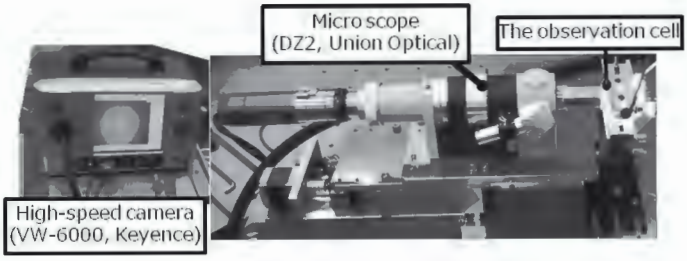


**Figure 2.11** Measuring equipment of the microscopic electrophoresis.

**Figure 2.12** Bubble size measurement.

The size of the microbubbles used for calculation of the ζ-potential is 20–30 μm, and it obtained directly from the picture acquired on the ζ-potential measurement as shown in Fig. 2.12. The ζ-potential

of the polystyrene particle was measured with this measuring method and the commercial measuring device (ζ-potential measuring device by Otsuka Electronics), the result was compared and the validity in this measuring method was checked.

#### *2.3.2.2.2 Calculation method of ζ-potential*

The ζ-potential can be obtained by observing and measuring the moving rate (electrophoresis rate) of the particles (microbubbles) according to the given voltage slope and using the Smoluchowski equation (Eq. 2.1) in the case of using microscopic electrophoresis [3]. In this equation, $Z$ is ζ-potential, $n$ is viscosity of the solvent, $u$ is electrophoresis rate and $e$ is dielectric constant of the solvent.

$$Z = \frac{nu}{e} \tag{2.1}$$

However, when the voltage is applied to the observation cell, not only the particles (microbubbles) of a measuring object but also an internal liquid will flow in response to the influence of the voltage, and the electrophoresis rate of the particles (microbubbles) obtained by actual measurement become an apparent rate [4]. When quartz is used for the observation cell under these pH conditions, the flow of the internal liquid is almost negligible since the isoelectric point of the quartz is between pH 2 and 3.

### 2.3.2.3 Results and discussion

#### *2.3.2.3.1 The ζ-potential of polystyrene particles*

The polystyrene particles were measured in pH 3 using both the microscopic electrophoresis and the ζ-potential measuring device, and the result were compared. The results are shown in Fig. 2.13. In this figure, a horizontal axis indicates the ζ-potential (mV), and the vertical one indicates the distance from the centre of the observation cell in the depth direction. Zero means the centre of the cell.

As a result of measurement, it has checked that the ζ-potential measured by both the techniques of the polystyrene particle

were almost the same value, which were between −20 mV and −10 mV.

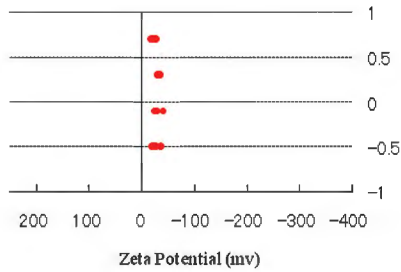


(a)

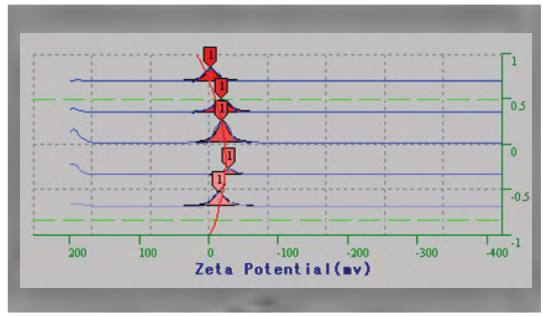


(b)

**Figure 2.13** The ζ-potential measurement results of the polystyrene particles. (a) The results of the microscopic electrophoresis. (b) The results of the ζ-potential measuring device.

#### *2.3.2.3.2 The ζ-potential of the air and argon gas microbubbles*

The measurement results of the air and argon gas microbubbles in pH 3 are shown in Fig. 2.14.

As the measurement results shown in Fig. 2.14, both the ζ-potentials of the air and argon gas microbubbles were in the range of 10–20 mV. This result is corresponded with the measurement result of the ζ-potential of air microbubbles by Takahashi. Under the conditions of pH 3, any difference of the ζ-potential was not observed in the microbubbles of the air and the argon gas.

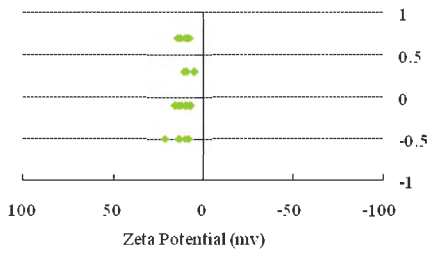


(a)

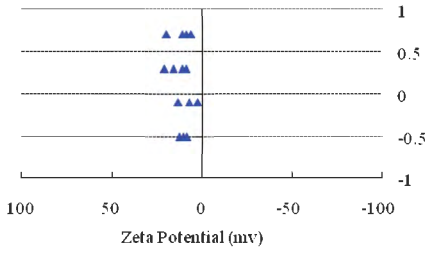


(b)

**Figure 2.14** The measurement results of the ζ-potential of the microbubbles in pH 3. (a) The ζ-potential of the air microbubbles. (b) The ζ-potential of the argon gas microbubbles.

### 2.3.2.4 Summary

The ζ-potential of the microbubbles of the argon gas was measured, and the behaviour was investigated. As a result, the difference was not observed in the ζ-potential of the microbubbles of the air and the argon gas under the conditions of pH 3. Still only one condition of the ζ-potential under the conditions of pH 3 of argon microbubbles was measured. So, another measurement with other pH conditions and other gas will be performed in near future to elucidate the electrification state of the surface of the microbubbles.

## References

1. Takahashi M (2005) The ζ Potential of Microbubbles in Aqueous Solutions: Electrical property of the gas-water interface, *J Phys Chem B*, **109** (46), 21858–21864.

2. Kitahara (1995) *Zeta Potential*, Scientist Press Co. Ltd. (in Japanese).
3. Furusawa (2004) Zeta(ζ)-potential measurements, *Bunseki*, **5**, 247–254 (in Japanese).
4. Mori (1980) A unified theory of determining the electrophoretic velocity of mineral particles in the rectangular micro-electrophoresis cell, *Fusen*, **27** (3), 117–126 (in Japanese).

### 2.3.3 Laser Diffraction/Scattering Method

**Mitsuru Maruyama**
*Global Application Development Center, Shimadzu Corporation, Kanagawa, Japan*
maruyama@shimadzu.co.jp

In recent years, microbubbles and nanobubbles have become a focus of attention, with applications such as the following:

i. Pharmaceuticals field
ii. Purification and cleaning
iii. Sterilization

In the pharmaceutical field, in particular, micro- and nanobubbles have been increasingly used for drug delivery systems and ultrasonic contrast media. In addition, while there are many precedents in the context of purification, applications to cleaning (particularly the cleaning of electronic equipment) remain forthcoming.

One of the significant factors determining the cleaning efficacy and other characteristics of these bubbles is their particle size distribution. Although a variety of methods are used for equipment for measuring particle size distributions, analysers using the laser diffraction/scattering method feature a number of benefits. These include a short measurement time (a few seconds to a few dozen seconds), a wide measurement range (a few dozen nanometres to several millimetres), good reproducibility and simple operability. As a result, through the 1990s, this type of particle size analysers became the norm. At first, the focus was on wet measurements, in which particles are suspended in a liquid. However, dry measurements, in which particles are in a gaseous phase, are now also performed. Recently, micro and nanobubble measurements have also become available, thereby making strides towards an epoch-making

methodology, completely distinguished from conventional particle size analysers by the breadth of applicable fields.

In terms of basic principles, micro- and nanobubble measurements use a simple method, in which the particles are exposed to a laser beam, and the particle size is specified from the scattered light generated as a result, using the dependence of particle size on the spatial intensity distribution pattern. Applications of this method are subsequently expected in a variety of fields. In addition, although a red laser is conventionally used as the light source, there are now also analysers that use short wavelength (blue) light sources, or even shorter ultraviolet lasers so as to enable the measurement of tinier particles, thereby extending the measurement range.

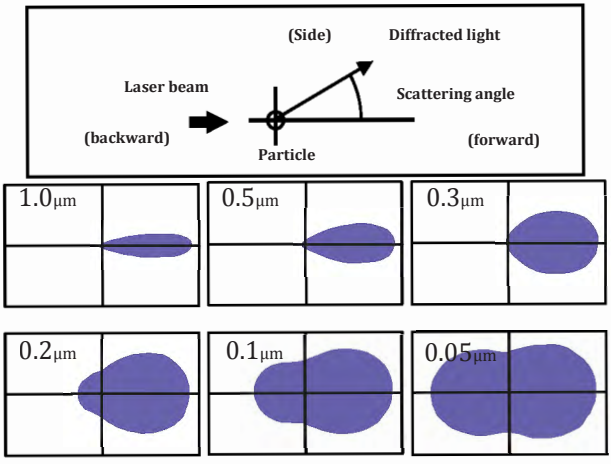


**Figure 2.15** Relationship between particle size and light intensity distribution pattern for scattered light.

### 2.3.3.1 Measurement principles

When particles are exposed to laser light, scattered light is emitted from the particles. This spatial scattered light intensity distribution pattern (the change in scattered light intensity in accordance with the scattering angle) changes in accordance with particle size as shown in Fig. 2.15. For example, scattered light emitted from 5 μm particles is concentrated in the forward direction. As the particle size becomes smaller, the angle of the scattered light emitted becomes larger, and when the particles are 0.3 μm or smaller, the

light scattered to the sides and backwards also becomes stronger. Furthermore, when the size drops to 0.1 μm, the intensity of the light scattered in the backward and forward directions becomes essentially the same. In this way, since the scattered light's light intensity distribution pattern changes in accordance with particle size, it conversely becomes possible to specify the particle size from the light intensity distribution pattern.

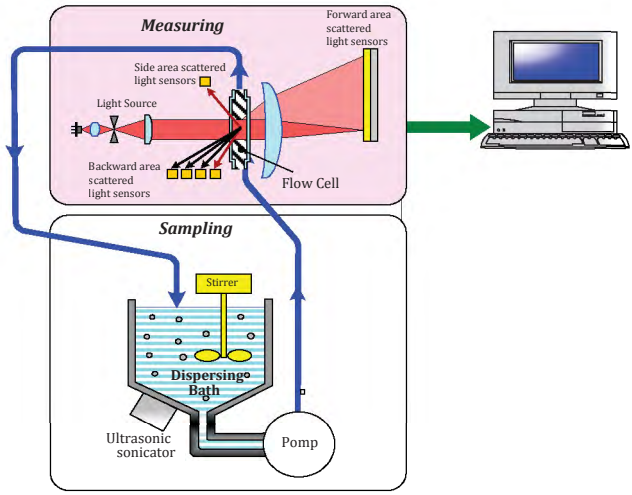


**Figure 2.16** Typical system configuration.

### 2.3.3.2 System configuration

In actual measurements, targets are groups of particles consisting of a number of particles of different sizes, which are dispersed in liquid or gas. If a group of particles is exposed to laser light, the scattered light emitted from the group of particles will be a superposition of the scattered light generated by the individual particles. A typical system configuration is shown in Fig. 2.16. Basically, it consists of an optical system (scattered light detector), a dispersion bath and a processor. The laser beam generated by the laser light source is converted to a slightly wider beam using the collimator lens and is then shone on the group of particles in a cell with a light path length of a few millimetres. The suspension filling the dispersion bath is circulated by a circulation pump. The light scattered in the forward direction is condensed by the lens and is united into a ring-shaped diffracted/scattered image on the detecting plane at the focal distance.

This is detected by ring sensors with detector elements arranged in concentric circles. Light scattered to the sides and backwards is detected by the side scattered light sensor and backscattered light sensors, respectively. In this way, light intensity distribution data is obtained by detecting the light intensity distribution pattern using a variety of detector elements.

### 2.3.3.3 Calculating the particle size distribution

The diffraction/scattering phenomenon due to the group of particles can be represented by the following (vector and matrix) equation:

$$\mathbf{s} = \mathbf{Aq}, \tag{2.2}$$

where

$$\mathbf{s} = \begin{bmatrix} s_1 \\ s_2 \\ \vdots \\ \vdots \\ s_m \end{bmatrix} \qquad \mathbf{q} = \begin{bmatrix} q_1 \\ q_2 \\ \vdots \\ \vdots \\ q_n \end{bmatrix} \tag{2.3}$$

$$\mathbf{A} = \begin{bmatrix} a_{1,1} & a_{1,2} & \cdots & \cdots & a_{1,n} \\ a_{2,1} & & & & \vdots \\ \vdots & & a_{i,j} & & \\ & & & & \\ \vdots & & & & \vdots \\ a_{m,1} & \cdots & & \cdots & a_{m,n} \end{bmatrix} \tag{2.4}$$

Here, "$s$" is the light intensity distribution data (vector). The elements "$s_i$" ($i$ = 1, 2, … $m$) are the light intensity (incident light quantity) detected by the various detection elements in the forward scattered light sensor and by the side scattered light sensor and backscattered light sensors. "$q$" is the particle distribution (frequency distribution %) vector.

The particle size range targeted for measurement (maximum particle size: $x_1$, minimum particle size: $x_{n+1}$) is divided into "$n$" segments, and the respective particle size sections become [$x_i$, $x_{i+1}$] ($j$ = 1, 2, … $n$). The "$q$" elements "$q_j$" ($j$ = 1, 2, … $n$) are the particle

quantities corresponding to the particle size sections $[x_i, x_{i+1}]$. Normally, a volumetric standard is used:

$$\sum_{j=1}^{n} q_j = 100\% \tag{2.5}$$

In other words, the data are normalised so that the total will equal 100 %.

"**A**" is the coefficient matrix for converting the particle distribution "*q*" (vector) to the light intensity distribution "*s*" (vector).

In terms of the physical meaning, the elements in "*A*", "$a_{i,j}$" ($i = 1, 2, \ldots m, j = 1, 2, \ldots n$), are the incident light quantity corresponding to the "*i*th" element of scattered light from the group of particles with the unit particle quantity belonging to the particle size section $[x_i, x_{i+1}]$. In other words, the numerical matrix "**A**" represents the very scattering phenomenon itself due to the group of particles. The value of "$a_{i,j}$" can be theoretically calculated in advance. This calculation uses Fraunhofer diffraction theory if the particle size is substantially larger than the wavelength of the laser light (10 times or more). However, for regions smaller than this, it is necessary to use Mie scattering theory. Fraunhofer diffraction theory can effectively be considered an excellent approximation to Mie scattering theory for very small-angle scatter in the forward direction when the particle size is significantly larger than the wavelength.

To calculate the elements in the coefficient matrix "**A**" using Mie scattering theory, it is necessary to set the absolute refractive index (complex number) for the particles and the media (liquid media) in which they are dispersed.

Thus, the following equation is obtained to find the least squares solution for the particle distribution (vector) "*q*" based on Eq. (2.2).

$$\mathbf{q} = (\mathbf{A}^T \mathbf{A})^{-1} \mathbf{A}^T \mathbf{s} \tag{2.6}$$

Note that "$\mathbf{A}^{\mathrm{T}}$" is the transposed matrix for "**A**", and "$(\ )^{-1}$" is the inverse matrix.

On the right side of Eq. (2.6), each of the light intensity distribution (vector) "**s**" elements is a numerical value detected with the forward scattered light sensor and side scattered light sensor. Also, the coefficient matrix "**A**" can be calculated in advance using Fraunhofer diffraction theory and Mie scattering theory. Accordingly, if Eq. (2.6)

is calculated using this already-known data, then the particle size distribution (vector) "$q$" is obtained.

Equation (2.6) is the basic method for calculating the particle size distribution from the light intensity distribution data with the laser diffraction/scattering method. However, just executing this equation as is leads to quite large errors, so in reality, the calculations performed on a computer are quite complicated and take into consideration a variety of conditions. In many cases, restrictions are added to the calculation, for example, to prevent the particle quantity from being a negative number, and to ensure that the particle size distribution is to some extent continuous.

### 2.3.3.4 System configuration for the measurement of microbubbles

The configuration of the system for measuring particle size distribution via the laser diffraction/scattering method has already been described, but there are some changes when microbubbles are targeted for measurement. This is because microbubbles and nanobubbles are very unstable and prone to collapse due to the particle characteristics. For this reason, as shown in Fig. 2.17, it is preferable that micro- or nanobubble size distribution measurements are made directly, without circulating the material. If the bubbles are still unstable, then to ensure stability, one method is to add a small amount of surfactant or ethanol.

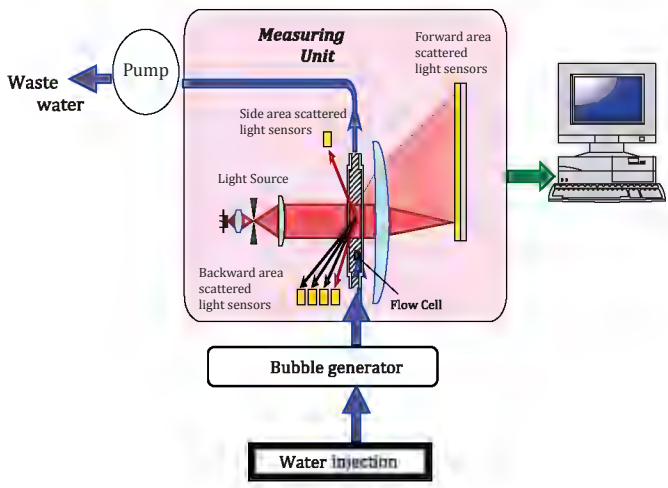


**Figure 2.17** System configuration for bubble measurements.

In terms of stabilizing and maintaining bubbles, it is also possible to measure them as is in a batch cell. Even in this case, inadvertent circulation may lead to bubbles being created or destroyed.

### 2.3.3.5 Measurement example

#### *2.3.3.5.1 Effectiveness of a dispersing agent*

Figure 2.18 shows the bubble size distributions obtained with the same bubble generator when they are generated with purified water only and with 1% ethanol added to purified water. It is evident that when the dispersing agent is added, the microbubbles stabilise, and small-particle bubbles are generated.

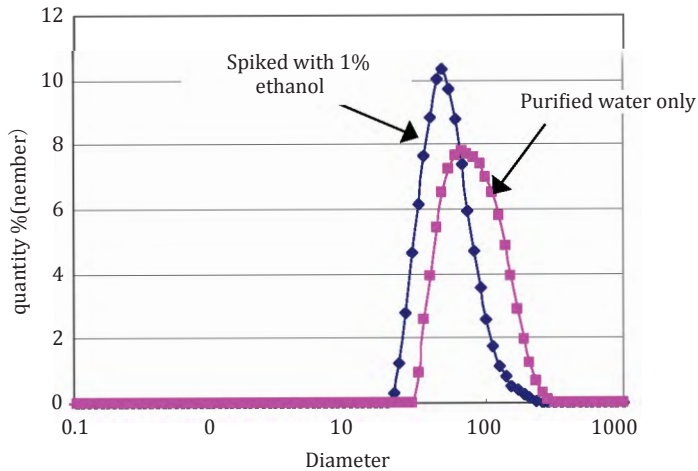


**Figure 2.18** Comparison of bubble size with purified water only and purified water spiked with 1% ethanol.

#### *2.3.3.5.2 Bubble generation*

The microbubble generation process was measured at 1 s intervals using two different pore bubble generation methods, and the respective 30 s measurement results are shown in Figs. 2.19 and 2.20. It is evident that with generation method A, microbubbles with a stable bubble size distribution are generated from the start, but with generation method B, stable bubble generation is not obtained. As in this case, since bubble generation may become unstable, measurements at short intervals must be considered as well.

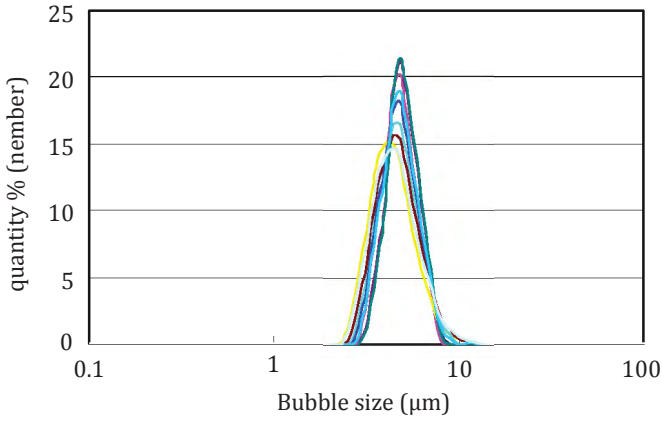


**Figure 2.19** Temporal development of bubbles generated with generation method **A**.

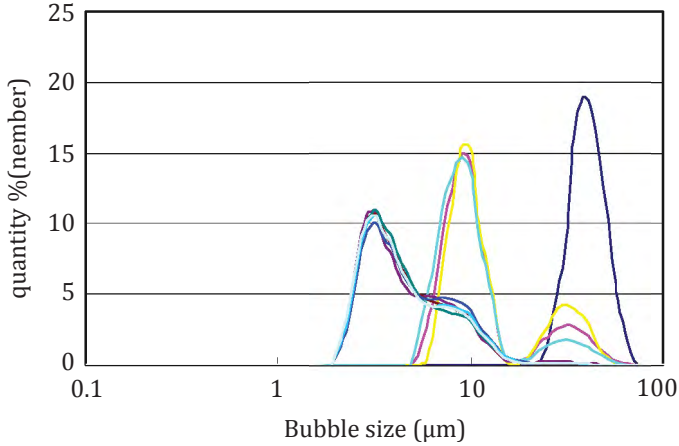


**Figure 2.20** Temporal development of bubbles generated with generation method **B**.

#### *2.3.3.5.3 Possibility of calculating the bubble concentration (Void ratio)*

Normally, with particle size distribution measurements using the laser diffraction method, as indicated in Section 2.3.3.3, not the absolute number of particles but the relative distribution is measured. However, it is possible to obtain the bubble concentration (void ratio) by measuring the scattered light intensity.

The scattered light intensity distribution, shown in Fig. 2.21 is the scattered light intensity detected with scattered light sensors arranged at a variety of angles. In normal measurements, this is used to check the optimal measurement concentration. However, if the particle quantity doubles, so too does the intensity, so it is possible to estimate the bubble concentration by comparison to a sample with a known concentration. Note that if the bubble size distribution differs significantly, then the scattered light intensity distribution diagram and intensity will change. Accordingly, calibration using a sample with similar particle sizes is necessary.

However, a general rule regarding this bubble concentration calculation is that the scattered light has not saturated the sensitivity of the light receiving sensor, so the limit concentration is about 0.1%.

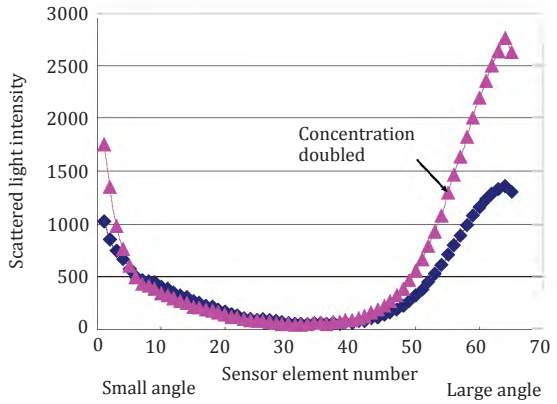


**Figure 2.21** Light intensity distribution data for scattered light changing in accordance with particle (bubble) concentration.

#### *2.3.3.5.4 Definition of particle quantities for bubble size distributions*

Standards of expression for investigating distribution quantities in bubble size distributions include particle number standards for investigating the number of particles and volumetric standards for investigating weights or volumes. Accordingly, even for the same aggregate of micro particles, bubble size distributions will differ considerably depending on the definitions of representative particle sizes (representing the size of the individual particles)

and particle quantity (number of particles, length, surface area and volumetric standard). JIS Z 8819-1 specifies how to represent these particle size analysis results. With the laser diffraction method, measurements are generally performed using a volumetric standard. However, when it is assumed that the particles are spherical, the conversion can be done with other standards. These conversions can be performed with the following equations:

Number of particle size divisions: $m$
Particle size: $X_j$ ($j = 1, 2, \ldots\ldots m+1$)
Average particle size for each section: $Z_j$ ($j = 1, 2, \ldots\ldots m$)
Difference % (volumetric standard): $q_j$ ($j = 1, 2, \ldots\ldots m$)
Difference % (particle number standard): $r_j$ ($j = 1, 2, \ldots\ldots m$)

$$y_j = \frac{\log_{10} x_j + \log_{10} x_{j+1}}{2}$$

$$z_j = 10^{y_j}$$

$$p_j = \frac{q_j}{(z_j)^3}$$

$$s = \sum_{j=1}^{m} p_j$$

$$r_j = \frac{p_j}{s} \times 100$$

For example, if 1 μm particles and 10 μm particles are considered, then even though the ratio will be 1:1 with a particle number standard, it will be 1:1000 with a volumetric standard. Accordingly, caution is needed, as a very different impression will result even for the same particle distribution measurement target depending on whether a volumetric standard or particle number standard is used.

In general, bubble size distributions are often expressed using either a particle number standard or a volumetric standard. Figure 2.22 shows the bubble size distributions using both the volumetric standard and particle number standard. Looking at the volumetric standard results, it is evident that approximately 20 μm microbubbles are generated. From the particle number

standard results, however, it is evident that a very large number of comparatively small 5 µm microbubbles are generated.

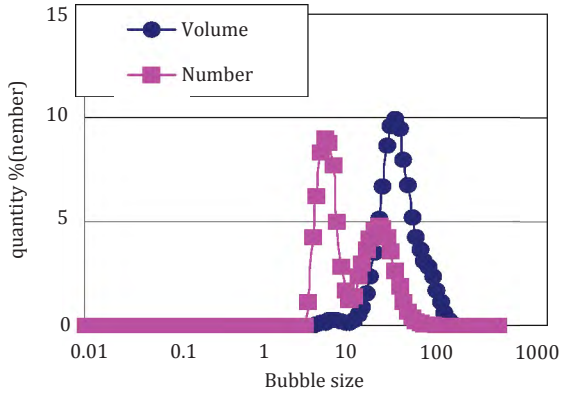


**Figure 2.22** Difference in the expression of bubble size distributions due to distribution standards (point of reference).

### 2.3.3.6 Considerations regarding measurement

#### *2.3.3.6.1 Considerations regarding the measurement path*

Bubbles are very unstable. Accordingly, stable measurements cannot be performed if pumps that produce pulses along the measurement path are used.

Also, bubbles may tend to adhere to oily components due to their characteristics, so stable measurements cannot be performed if hydrophobic materials are used in the measurement path.

#### *2.3.3.6.2 Considerations regarding the measurement concentration*

If the particle concentration is large, as shown in Fig. 2.23 light scattered from one particle will tend to shine onto other particles and be further scattered. This phenomenon is referred to as multiple scattering. In this case, the particles will tend to appear smaller than at appropriate concentrations. For this reason, while results will differ depending on the light path length (cell length) and particle size distribution, normally, a concentration less than a few 100 ppm is used. Recently, however, analysers have been developed that is capable of measuring even high-concentration samples on the order

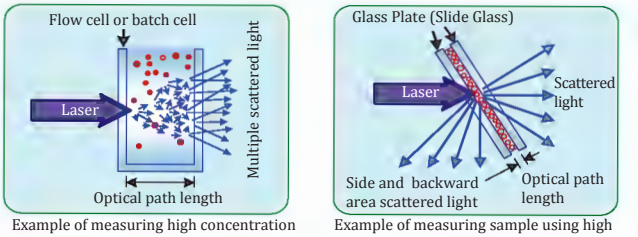


Example of measuring high concentration sample using standard method.

Example of measuring sample using high concentration sample measurement system.

**Figure 2.23** Approaches to high-concentration measurements.

of a few percent to 20% by volume, by making the light path length as short as possible.

On the contrary, the scattered light intensity becomes extremely small when the particle concentration is low, so the S/N ratio will drop, and accurate results will not be obtained. In this case, suggestions include increasing the laser light output or lengthening the light path length.

#### *2.3.3.6.3 Contamination of the optical system*

If the optical system becomes contaminated (particularly by the adhesion of contaminants to the cell), coherency will worsen due to light scattered by the adhering particles. Accordingly, there will be an impact on the particle size distribution even if blank calibration is performed. Also, bubbles may tend to adhere to contaminants due to their characteristics, leading particle sizes to appear large, so caution is needed.

## References

1. The Society of Powder Technology, JAPAN (ed) (1998) *Powder Technology Handbook*, 2nd ed, Nikkan Kogyo Shimbun Ltd.
2. The Society of Powder Technology, JAPAN (ed) (2000) *Terminology Dictionary of Powder Technology*, 2nd ed, Nikkan Kogyo Shimbun Ltd.
3. The Society of Powder Technology, JAPAN (ed) (1994) *Measurements, Techniques of Particle Diameter*, Nikkan Kogyo Shimbun Ltd., pp 145–167.

## 2.3.4 Electrical Sensing Zone Method (Coulter Counter)

**Yiming Yang**
*Micromeritecs Japan G.K., Kashiwanoha, Kashiwa, Chiba 277-0882, Japan*
yiming.yang@micromeritics.com

### 2.3.4.1 Introduction

Micro- or nanobubbles are expected to be applied in the field of various environmental, industrial, food, and the medical field. Generally, microbubbles and nanobubbles have been classified according to the bubble size, it is said that microbubbles are 10–100 μm, and nanobubbles are less than 1 μm. It is most important to measure the bubble size and the concentration for knowing the function of bubbles, electrical sensing zone method can be used on the measuring the bubble size and the concentration as a standard measurement method. It is the best way as the highest accuracy measurements of bubble size distribution and the concentration, since this method is measuring the volume and number of individual bubble.

Electrical sensing zone method was developed as a technology that measures simultaneously the number and the size of the particles dispersed in the electrolysis solution by Wallace Coulter late in the 1940s, and it was also called the Coulter principle. Initially, the instrument based on this technology has been used to facilitate the analysis of blood cells; it was also a very useful tool in industrial applications. Electrical sensing zone method are described in international standards and national standards in many measuring instruments, from the height of the measurement accuracy, as a criterion in the evaluation of particle size measurement technology, and are frequently used.

This chapter introduces the pretreatment, the display of the important matter, the measurement result, the statistics analysis and the measurement procedure, etc. for measuring the size distribution of the microbubbles and nanobubbles more correctly using this method; at the same time, it explains the newest technology of the electrical sensing zone method.

### 2.3.4.2 Principle

#### *2.3.4.2.1 Electrical sensing zone method*

By the particle size distribution measuring method, called an electrical sensing zone method, the wall which has one penetrated aperture is established into the electrolysis solution, which particles are distributing, an electrode is put on both sides and constant current is sent through the aperture. When particles pass aperture with an electrolysis solution by attracting the electrolysis solution, which dispersed particles by a certain fixed power of absorption from the inner side of fine pores, only the quantity in which the electrolysis solution in fine pores is equivalent to the volume of particles decreases, and the electrical resistance of aperture becomes larger in proportion to this eliminated amount of electrolysis solutions. The current flowing into aperture is not concerned with existence of particles, but the amount of voltage change is proportional to the amount of change of the electrical resistance of aperture. The volume of particles can be measured from the amount of voltage change, and it can ask for the diameter of a ball equivalent of particles from this volume; it can display the diameter distribution of a bubble. Moreover, the bubble concentration in suspension can be quantitatively measured by calculating a voltage change (electric pulse) number by the number with which the bubble passed fine pores counting and attracting fixed capacity (Fig. 2.24).

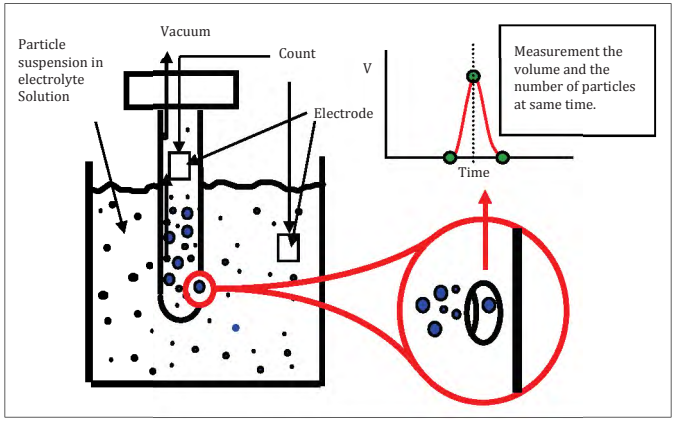


**Figure 2.24** The principle of Electrical Sensing Zone method.

In international standard ISO 13319 "Determination of particle size distributions—Electrical sensing zone method", the guidance about particle size distribution measurement of the particles using Coulter principle is provided.

#### *2.3.4.2.2 Equivalent sphere diameter*

Although it has measured the true volume of particle (bubble) each, since it is common to denote particles (bubble) by a diameter as for an electric detection belt method when applying to the industrial field, it changes particle (bubble) volume into the diameter (ESD) of a ball equivalent (Fig. 2.25). In this case, the diameter of a particle (bubble) turns into a diameter of the ball of the same volume as that particle. In the case of the method of computing from the two-dimensional data (area) of particles, such as an image analysis method, two or more values will be made from one particle (bubble) with a detection position. Temporarily, when the particles (bubble) of the same triangular pyramid are measured, the value of an image analysis method varies, but the method of measuring volume is not subject to the influence of the measurement direction.

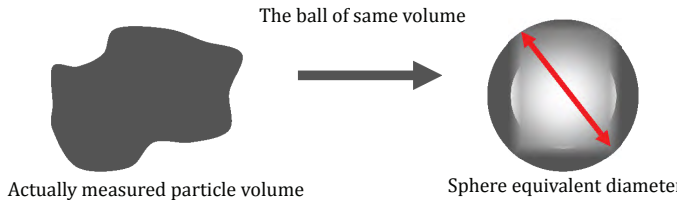


**Figure 2.25** Equivalent sphere diameter.

### 2.3.4.3 Calibration

Particle volume is measured using known standard particles, and it asks for this proportionality factor. This the operation of a series of is calibrating of equipment. Like a formula (2.7), particle volume ($V_p$) is proportional to the electric pulse ($\Delta V$ ) obtained when particles pass an aperture.

$$\Delta V = I\Delta R = I\frac{\rho^0}{S^2}V_p \tag{2.7}$$

where $\Delta V$ is the electric pulse, $I$ is the current value, $S$ is the cross-sectional area of aperture, $\rho^0$ is the resistance of

electrolysis solution and $V_p$ is the particle volume, ($I$) of formula (2.7) is a constant current value actually passed, and the value of ($\rho^0/S^2$) changes in an electrolysis solution, the diameter of an aperture, the form of an aperture, etc. Generally, ($K_d$) is denoted by formula (2.8) and connected with resistance ($\rho^0$) of current value ($I$), the cross-sectional area ($S$) of an aperture and an electrolysis solution.

$$K_d \propto \frac{S^2}{I \cdot \rho^0} \tag{2.8}$$

In actual calibrating, it measures using the standard particles (monodisperse particle) which the diameter of a particle (or volume) understands correctly, and determines ($K_d$). Each diameter of a particle ($d$) is calculated by formula (2.9) by determined ($K_d$).

$$d = K_d \sqrt[3]{V_p} \tag{2.9}$$

#### *2.3.4.3.1 Selection of standard particles*

It is necessary to choose calibrating particles according to the diameter of an aperture to be used, and they usually use the standard particles from 10% to 20% of an aperture diameter. The optimal calibrating refers to the calibrating particles which Table 2.1 recommends.

**Table 2.1** The optimal calibrating particles is recommended

| Aperture diameter (μm) | Range of standard particle diameter (μm) | Diameter of value of standard particles to recommend (μm) |
|---|---|---|
| 20 | 2–4 | 2 |
| 30 | 3–6 | 3 |
| 50 | 5–10 | 5 |
| 70 | 7–14 | 10 |
| 100 | 10–20 | 10 |
| 140 | 14–28 | 20 |
| 200 | 20–40 | 30 |
| 280 | 28–56 | 30 |
| 400 | 40–80 | 43 |
| 560 | 56–128 | 65 |
| 1000 | 60–150 | 90 |
| 2000 | 90–260 | 90 |

### 2.3.4.4 Sample measurement

Unlike measurement of particles, it is not necessary to pretreat the bubble ultrasonically. Creation of measurement liquid is completion as bubble water is mixed with the electrolysis solution used for an electric detection belt method about measurement of nanobubbles. The rest is set in a measuring device and becomes pushing the start button of equipment. When measuring quantitatively, it is necessary to make regularity the ratio (1:9), which an electrolysis solution mixes with nanobubbles water and measures a fixed quantity in measurement mode to the measuring device side.

Moreover, when measuring microbubbles, since they are unstable, the microbubbles must measure the prepared measurement liquid promptly; and fixed-quantity measurement is the same method as nanobubbles, sets to 1:9, the ratio which an electrolysis solution mixes with bubble water, and measures a fixed quantity in measurement mode to the measuring device side. An example of the optimal diameter of a bubble, an aperture tube and dilution magnification, and a time-base range is shown in Table 2.2.

**Table 2.2** Sample and use aperture, dilution factor, measurement range

| Sample | Aperture diameter (μm) | Dilution factor | Measurement range (μm) |
|---|---|---|---|
| Nanobubble | 20 | 10 times | 0.4–12 |
| Microbubble (below 10 μm) | 50 | 10 times | 1–30 |
| Microbubble (above 10 μm) | 200 | 10 times | 4–120 |

#### *2.3.4.4.1 Measurement procedure of nanobubbles*

Since a measurement procedure has some differences depending on the model, a concrete procedure is carried out to my having each manual referred to and describes only a fundamental procedure here. The aperture of 20 μm is usually used for nanobubbles measurement.

1. A measuring instrument and the computer for control are turned on, dedicated software is started and it checks that operation of each part is normal.
2. An aperture suitable for a sample is attached, and an electrolyte solution is filled to instrument.

3. Each conditions (counting for bubble, the current value to an aperture, an amplification rate, a calibration factor, calculation method etc.) for measuring are set up.
4. A 90 mL electrolyte solution is put into a measurement container (round-bottom beaker), a container is installed in the predetermined position of a measuring device and it agitates at a speed suitable for a sample.
5. The bubble of 10 mL is extracted and is supplied to the prepared beaker.
6. Measurement is started in mode (100 μL) of volume.
7. The diameter distribution of a bubble and a statistics value are calculated. Various data are printed and saved.

#### *2.3.4.4.2 Measurement procedure of microbubbles*

The aperture of 50–200 μm is usually used for measurement of microbubbles.

1. A measuring instrument and the computer for control are turned on, dedicated software is started and it checks that operation of each part is normal.
2. An aperture suitable for a sample is attached, and an electrolyte solution is filled to instrument.
3. Each conditions (counting for bubble, the current value to an aperture, an amplification rate, a calibration factor, calculation method etc.) for measuring are set up.
4. A 90 mL electrolyte solution is put into a measurement container (round-bottom beaker), a container is installed in the predetermined position of a measuring device, and it agitates at a speed suitable for a sample.
5. Using a syringe as much as possible with a large exit, the bubble of 10 mL is extracted and is supplied to the prepared beaker.
6. Measurement is started in mode (100 μL) of volume.
7. The diameter distribution of a bubble and a statistics value are calculated. Various data are printed and saved.

### 2.3.4.5 Display and statistics analysis of a measurement result

In instrument in recent years, in order to measure the volume of a bubble by a multi-channel, the diameter distribution of a bubble is obtained in real time. Since the bubble diameter and

number of a ball are calculated, number standard distribution is correctly convertible for volume standard distribution. Moreover, since the number of channels is changeable, the optimal result can express as the equipment that carries the digital pulse processing capability at any time if needed. In order to measure the diameter distribution of a bubble by high resolution, it is desirable to narrow a time base range or to increase the number of channels.

#### *2.3.4.5.1 Display of the size distribution of a bubble*

Size distribution of a bubble recommends what is usually displayed by the number distribution. However, when conducting an experiment which a bubble destroys by giving an ultrasonic wave to a bubble, in order to display bubble distribution, it recommends using number distribution and volume distribution. As shown in Fig. 2.26, while there was a peak of 0.5–0.8 μm before ultrasonic irradiation in $5.2 \times 10^6$ number/mL, after ultrasonic irradiation was be to $1.7 \times 10^6$ number/mL, and the nanobubbles of the 0.5–0.8 μm decreased, but the total volume of a bubble changed from $7.6 \times 10^5$ μm$^3$/mL to $6.0 \times 10^5$ μm$^3$/mL in the same range of volume distribution, and it has the almost same volume. It was proved that the nanobubbles were united according to an ultrasonic wave. Therefore, it is necessary to use the number distribution and volume distribution for display of the bubble size distribution when the nanobubbles are processed by ultrasonic irradiation, etc.

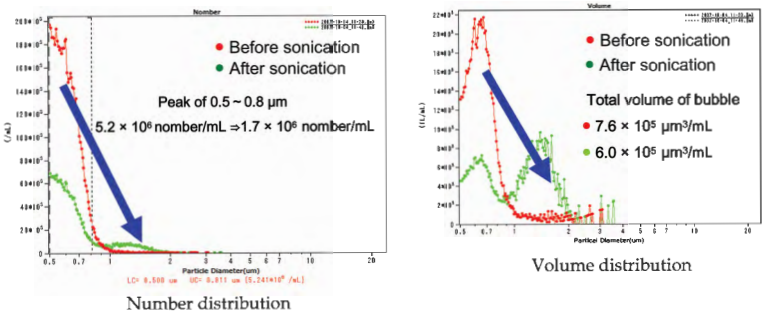


**Figure 2.26** Distribution before and after supersonic. (Data are offered from Kyowakisetsu Inc.)

#### *2.3.4.5.2 Statistics of the size distribution for bubble*

Statistics and a size distribution display recommends taking the statistics of number distribution and volume distribution, respectively. Usually, the concentration of a bubble is computed by number distribution, and the sum total volume of a bubble is calculated by volume distribution. Moreover, it is desirable to ask also for the central value (the median diameter and the modal diameter) of each distribution and the diameter of an average bubble. With commercial equipment, various statistics calculations are included in software, and a statistics value can be obtained only by menu selection.

#### *2.3.4.5.3 Report and record for result*

As for the measurement result of the bubble by electrical sensing zone method, it is desirable to write the matters following at least in a report. Moreover, if it is possible, it is desirable to make digital pulse shape data record with the diameter data of a bubble.

1. Sample information
2. Procedure in dispersion of sample, method, etc.
3. Starting time, measuring time
4. Used aperture diameter
5. Setting conditions of instrument (current of aperture, amplification rate, calibration factor $K_d$, etc.)
6. Frequency and cumulative size distribution of bubble (number standard, volume standard or area standard)
7. Frequency list of the bubble size distribution, the statistics result of the bubble size distribution

### 2.3.4.6 Notes on measurement

#### *2.3.4.6.1 Removal of electric noise*

It is desirable to install the instrument in environment clean in electromagnetism and to attach a noise filter to the power supply by a case. It is necessary to ensure ground installation of main part. Since a 20 μm aperture is used for measurement of a nanobubble, cautions are required for especially an electric noise.

#### *2.3.4.6.2 Contamination influence form solution*

By electrical sensing zone method, although it is the feature to survey the number absolutely of bubble, compared with other measuring methods, the influence of contamination is also high, and cautions are required for mixing of a foreign substance enough in the process of measurement. Washing of tools (beaker, pipette, aperture, etc.) and management of electrolysis solution require cautions enough. The washed tool is an electrolysis solution to be used and is prewashing. Moreover, since even the air bubbles in electrolysis solution may be measured as contamination, when pouring an electrolysis solution into a measurement beaker, it puts in slowly so that a bubble may not form. Since the dissolved gas becomes the air bubble while measuring, it becomes a factor with error when the electrolysis solutions of private manufacturer are used, it is necessary to carry out decompression degassing of the solution beforehand. Decompression degassing is unnecessary when using the exclusive electrolysis solution on the market.

#### *2.3.4.6.3 Washing aperture*

At the comparatively small aperture (less than 100 μm), fine pores have easily got blocked with foreign substance particles. In order to prevent this, it is necessary to soak the aperture, which is not used in detergent, it is desirable to also soak the aperture currently used in the electrolysis solution for measurement. If the latest instrument carries the camera that observes the blocked aperture, taking out automatic warning when the aperture will be blocked, and there is a function to remove a jam automatically with contrary pressure. In addition, the block of aperture is removable by one of the methods below.

1. Adverse pressure: Pour liquid in the pressure from the opposite direction to the aperture until it cancels the block.
2. Heating: Liquid is boiled at heating by current of aperture, then the block can be removed.
3. Brushing: It is possible to clear blockages from the aperture tube using the short brush of hair. It is necessary to warn against doing damage to the aperture tube at this time.

4. Clearing blockages by ultrasonic: Where an electrolyte solution is filled to the aperture tube, the aperture portion is dipped in ultrasonic bath of a low power for about 1 s. This operation is repeated if needed. Although this method is effective, ultrasonic damage may be done to the aperture tube, it is necessary to carry out carefully.

Caution: It is better not to use ultrasonic cleaning for the aperture tube of less than 50 μm size.

### 2.3.4.7 Conclusion

The size distribution measuring method of the bubble is measuring the bubble size using various principles from a dynamic light scattering method to a high-speed image analysis method or the laser diffraction scattering method. However, these are measuring the bubble by two dimensions, and only the electrical sensing zone method is carrying out three-dimensional measurement, which surveys volume of the bubble. Thereby, there is no influence of the detection direction, and it can measure a slight volume change of the bubble by precise and high resolution. Since a bubble can be quantitatively measured while measuring the volume of the bubble, in order to measure the number and the size distribution of micro- and nanobubbles, the electrical sensing zone method is the most outstanding measuring method.

Moreover, since international standards particles are united with the prototype meter which is a standard of length, if a measuring device is proofread using this, the traceability, which used the diameter of a ball equivalent as the base, is also securable.

## References

1. Measurement technology for particle size (Nikkan Kogyo Shimbun Ltd, 1994).
2. The light scattering diffraction particle-size-distribution measuring method of laser + polarization (Optical alliance 2000.8).
3. Application of the Electrical Sensing Zone method particle-size-distribution measurement machine in quality control of CMP slurry (Tribology planarization technology for CMP in semiconductor 2007.11).

4. The Association of Powder Process industry and Engineering, Japan (1994) Particulate engineering-the foundation of distribution and application.
5. ISO 13319 Determination of particle size distributions—Electrical sensing zone method.

## 2.3.5 Measurement of Size and Zeta Potential of Nanobubbles

**Kazuhiro Nakashima**
*Sysmex Corporation, Kobe 651-2271, Japan*
Nakashima.Kazuhiro@sysmex.co.jp

### 2.3.5.1 Introduction

There are various types of nanobubble generation systems that include ultrasonic and gyration, pressure dissolution, detailed hole by enclosing the gas in a solvent. Size and zeta potential of nanobubbles can be controlled by changing electrolyte concentration and pH in the solvent. The Zetasizer Nano of Malvern Instruments (Fig. 2.27) can measure the size and the zeta-potential of nanobubbles by using the dynamic light scattering (DLS) method and the laser Doppler method. This paper addresses the measurement principle and the function, the example of nanobubbles measurement with the Zetasizer Nano.

**Figure 2.27** Zetasizer Nano of Malvern instruments.

### 2.3.5.2 Size measurement

In DLS, the diameter of particles is calculated by measuring Brownian motion of particles in a solvent. The Brownian motion is the random motion of particles, which happened by the collision of the solvent molecules and the particles; it is known that small particles move quickly, and large particles move slowly in a solvent.

The size of the particle is given by the Stokes–Einstein equation Eq. (2.10) with the diffusion coefficient. In DLS, the diffusion velocity of the particles by Brownian motion is measured. This is performed by measuring fluctuation of scattering light intensity using the suitable optical device. Figure 2.28 shows correlation curve of the typical size of particles. Since the Brownian motion of large particles is slow and the fluctuation of scattering light intensity changes slowly, the correlation will persist for a long period of time. Moreover, since the Brownian motion of small particles is fast and the fluctuation of scattering light intensity changes quickly, the correlation will reduce for a short period of time. The diffusion coefficient of particles is calculated by the inclination of the correlation curve, and the diameter of particles is computed using the Stokes–Einstein equation (Eq. (2.10)). Moreover, it is shown that the monodispersity of particles is the rapid inclination of the correlation curve. It is shown that the polydispersity of particle is the slow inclination of the correlation curve. The diameter of particles is calculated by the correlation function using various algorithms.

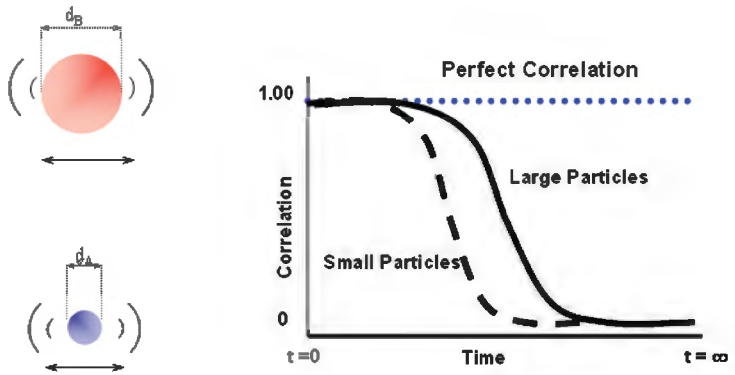


**Figure 2.28** Correlation curve of the typical size of particles.

1. Cumulant analysis: The method of estimate of Z-Average (mean diameter) and polydispersity index (PDI) by applying the single exponential function to the correlation function (ISO13321 Part 8).
2. Non-negative least squares (NNLS) analysis: The method of acquire of the diameter distribution by applying the plural exponential functions to the correlation function.

The diameter distribution of particles is the plot of the relative intensity of the scattering light of the various size particles.

$$d(H) = \frac{kT}{3\pi\eta D} \tag{2.10}$$

$d(H)$ = hydrodynamic diameter
$D$ = translational diffusion coefficient
$k$ = Boltzmann's constant
$T$ = absolute temperature
$\eta$ = viscosity

#### 2.3.5.3 Zeta potential measurement

Increasing the charge of the particle surface, the distribution of ion surrounding the interface domain is affected, and, as a result, the concentration of opposite ion (the electric charge of particles and opposing electric charge ion) will rise near the particle surface. For this reason, the electrical double layer is formed in the surroundings of each particles. Moving the particles by an electric field, the ion in an electric double layer move with the particles, and the potential of outside of the electric double layer is the zeta potential. Figure 2.29 shows schematic representation of zeta potential. The zeta potential is an index of the disperse stabilisation in colloid system. The zeta potential of all suspended particles—positive/negative—when one of big values are shown, the restitution between particles is large and the diameter distribution of particles is stabilised over a long period of time.

Moreover, if the zeta potential of particles is low, the restitution between particles will become small and aggregation of particles, adhesion on a container will occur. If the electric field is impressed, particles can be drawn near to the electrode of an opposite mark, the viscous force influence to particles resist this motion easily. If

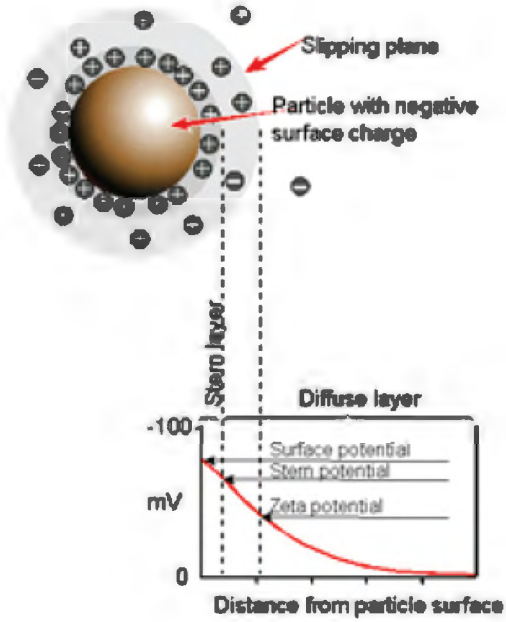


**Figure 2.29** Schematic representation of zeta potential.

two power of being opposed to each other reaches equilibrium, the motion of particles become uniform velocity. The factors that influence uniform velocity are the electric field intensity and the voltage slope, the dielectric constant of a solvent, the viscosity of a solvent and the zeta potential.

The relation between the zeta potential and the electrophoretic mobility of particles in an electric field is shown by the following Henry equation (Eq. (2.11)).

$$U_E = \frac{2\varepsilon Z f(\kappa a)}{3\eta} \tag{2.11}$$

$U_E$ = electrophoretic mobility
$Z$ = zeta potential
$\varepsilon$ = dielectric constant
$\eta$ = viscosity
$f(\kappa a)$ = Henry's function
$\kappa^{-1}$ = termed the Debye length
$a$ = radius of particle

The electrophoresis measurement of zeta potential is the general method used to the middle electrolytic concentration of aquarius solvent. In this case, $f(\kappa a)$ set to 1.5, and the formula is called Smoluchowski approximation. The Zetasizer Nano measures by combining M3-PALS technology to the laser Doppler method.

Mixed-mode measurement is the method of changing the reversal cycle of the electric field which is fast-field-reverse (FFR) and slow-field-reverse (SFR) (Fig. 2.30). FFR can measure the electrophoretic mobility of particles without the influence of electric osmosis.

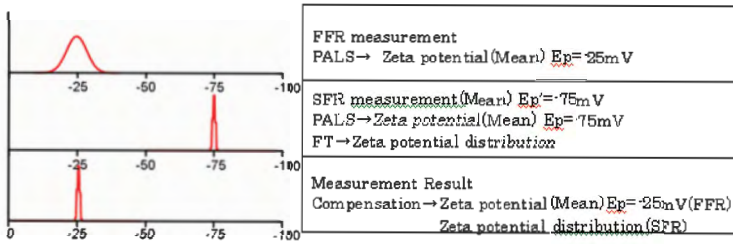


**Figure 2.30** Measurement process: series of FFR and SFR.

The Zetasizer Nano calculates the average of electrophoretic mobility by analysing the phase shift of scattering light pitch with the phase analysis light scattering (PALS) method for FFR. SFR can improve the resolution of the electrophoretic mobility, because there are also many amounts of samplings in the electric field and the electric osmosis is stabilised. Then, by conducting frequency analysis using Fourier conversion, while analysing the exact distribution of the electrophoretic mobility, the average of electrophoretic mobility is computed by the PALS method like FFR. Then, Zetasizer Nano calculates the exact distribution of the electrophoretic mobility by analysing the frequency with the Fourier conversion and computes the average of electrophoresis mobility with the PALS method of FFR.

The difference of the average of electrophoretic mobility computed by SFR and FFR is the speed of the electrical osmosis, and it can measure the zeta potential without the influence of an electrical osmosis by rectifying the exact distribution of the electrophoresis mobility obtained by Fourier conversion. PALS analyses the abnormal conditions of the pitch (phase shift) by the interference of reference light and scattering light (Fig. 2.31). In analysing the phase shift of scattering light pitch,

the electrophoretic mobility is correctly computed except for the factors (Brownian motion, particle sedimentation, the convection of suspension, etc.). The Zetasizer Nano detects in high sensitivity the electrophoretic mobility of the particles, which are the low-charge particle surface in a high-concentration electrolyte or non-polar solvent.

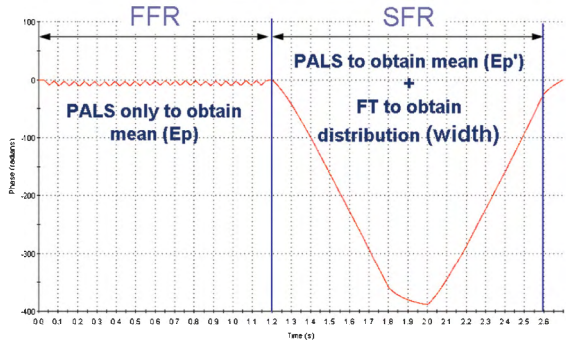


**Figure 2.31** Phase plot.

### 2.3.5.4 Nanobubble measurement

Figures 2.32 and 2.33 show the diameter and the zeta potential of the nanobubbles that are generated from the nanobubble generation equipment BUVITAS made from Kyowa corporation by using Zetasizer Nano ZS (green laser: the wavelength of 532 nm, the dip cell used). According to Fig. 2.32, it was thought that the correlation curve was the reliability data from the intercept of correlation coefficient showed high value near 1.0 and the high S/N ratio without the influence of the noise.

Moreover, since the correlation curve of attenuation intensity changed slowly, the correlation will persist for a long period of time. Z-Average (mean diameter) computed from the cumulant analysis was 168 nm, and PDI was 0.398 as the large size and polydispersity result.

The mean diameter and the distribution computed from the NNLS analysis showed that the main peak was 168 nm, and the half of width was 105 nm as comparatively broad distribution.

From the result of the cumulant analysis and the NNLS method, comparatively broad distribution ware obtained.

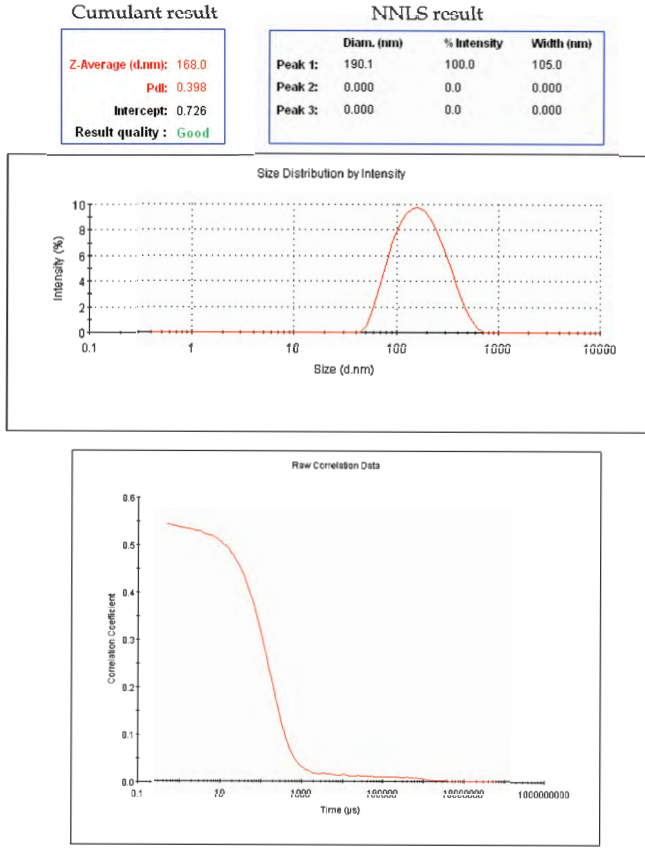


**Figure 2.32** Result of diameter distribution of nanobubbles (upper: distribution, lower: correlation curve).

According to Fig. 2.33, the reliability data were obtained because nanobubble followed the change of an electric field FFR and SFR and the phase was clear. It was obtained that the distribution of zeta potential was comparatively as sharp as the average of zeta potential was –13.7 mV and the standard deviation of zeta potential distribution was 2.93 mV.

Since there was no diameter parameter of particles in the Henry (Eq. (2.11)), the zeta potential distribution was comparatively sharp as the mobility of the particles in the electric field were gathered in spite of the diameter distribution was broad.

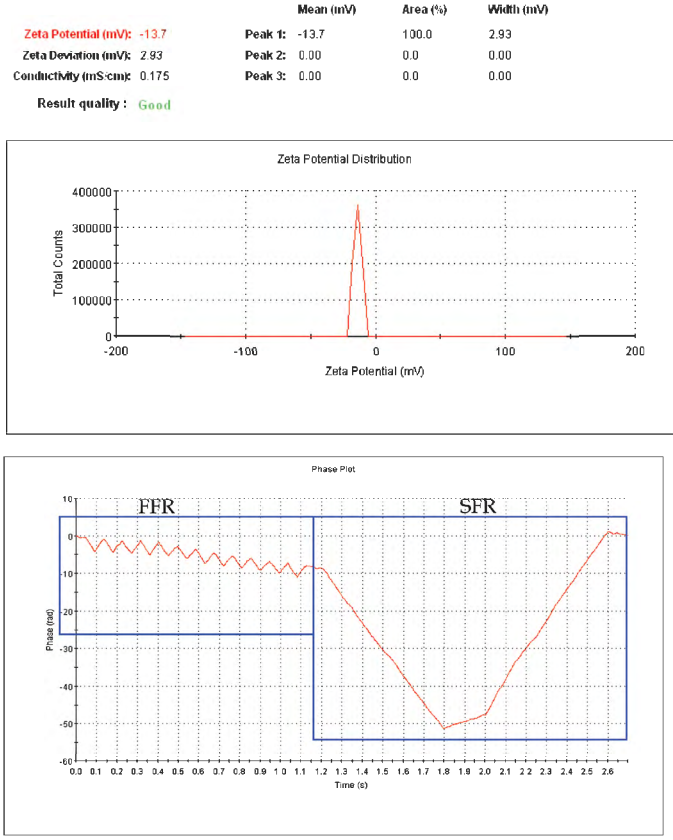


**Figure 2.33** Result of zeta potential of nanobubbles (upper: zeta potential distribution, lower: phase plot).

## 2.3.6 Particle Size Distribution of Nanobubbles by NanoSight System

**Ayako Irie**
*Advanced Technology Div. Quantum Design Japan, Tokyo, 171-0014, Japan*
irie@qdj.co.jp

The information of nanobubble (NB) size and concentration become important to verify the effect of NB. In existing systems, transmission electron microscopy, dynamic light scattering and laser diffraction system, it is difficult to measure the NB size and concentration at

the same time. Assumed size and concentration measurement of NB was performed using the "NanoSight system" which is able to track individual nanoparticles moving under Brownian motion and relates the movement to a particle size according to the following formula derived from the Stokes–Einstein equation. As a result, it checked that the model size of particle size distribution was 72 nm, and the total concentration was 3.28E8 particles/mL. From this result, it was suggested that it is possible to measure the size and concentration of NB using "NanoSight system". Therefore, initial studies using the NanoSight system would suggest that it is useful for NB generator's optimisation, NB's physical studies and so on.

#### 2.3.6.1 Introduction

Microbubble/nanobubble (NB) is of interest due to a specific ability which a bubble has, that is cleaning effect. Various application examinations are done in many kinds of business fields. However, scholarly knowledge is low, for this reason, this research is still developing. It is clear that the information of bubble size and concentration is very important to study the effect that bubble have, but the measurement method is not established.

There are already well-defined techniques for the analysis of nanoparticles. Transmission electron microscopy is used for observation of the particle shape and for measurement the size of the nanoparticles. This is not suitable to measure NB, as samples must be analysed in a reduced pressure environment. Therefore, particle size distribution system, this is the technology that considers that bubble is solid particles and measures them, is made available for measurement the NB size.

Particle size distribution system is developed to measure the particle size distribution of particles. That means the result from existing particle size distribution system is displayed "frequency". So, it cannot be counted the particle number directly, and this system needs to input a refractive index for every measurement particle. A refractive index has a close relation to density. There is a question: "May I use the refractive-index value of the gas in atmospheric pressure to a NB with unknown internal pressure?" When measuring known solid particles, it is satisfactory, but to measure a strange substance like an NB, it is necessary to pay attention to the input of physical properties information.

Dynamic light scattering (DLS): it is known the photon correlation method. Measure fluctuations within the scattered light intensity from a sample result from the Brownian motion of the particles within a sample. Application of the Stokes–Einstein equation relates the speed of particle movement to particle size in a sample of known viscosity and temperature. DLS performs well in a monomodal populations but is highly influenced by a small number of larger particles that scatter a disproportionately large amount of light compared with a smaller particle (light scatter is proportional to the ^6 of the radius in the Rayleigh regime).

It is thought that an NB, size is under 1000 nm, has distribution width, and exists in liquid. Moreover, in NB liquid, particulates other than the bubble, that is dirt, which arose at the time of bubble generation may be included. Thus, it is difficult to measure the actual size distribution and concentration of NB. We introduce measurement of an NB's size, concentration and zeta potential (ZP) using a "NanoSight system", which uses a unique technology called "Nanoparticle Tracking Analysis (NTA)".

### 2.3.6.2 About NanoSight

#### *2.3.6.2.1 Principles of operation*

NTA uses the properties of both light scattering and Brownian motion in order to obtain particle size distributions of samples in liquid suspension. A laser beam (of arbitrary wavelength but typically those available from laser diodes operating at 635, 532, 488 or 405 nm) is passed through a prism edged glass flat within the sample chamber. The angle of incidence and refractive index of the glass flat is designed to be such that when the laser reaches the interface between the glass and the liquid sample layer above it, the beam refracts to an intense low profile resulting in a compressed beam with a reduced profile and a high power density. The particles in suspension in the path of this laser beam scatter light in such a manner that they can be easily visualised via a long working distance, ×20 magnification microscope objective fitted to an otherwise conventional optical microscope objective onto which is mounted a charge-coupled device (CCD), Electron Multiplying Charge Coupled Device (EMCCD) or high-sensitivity Complementary Metal-Oxide Semiconductor (CMOS) camera, operating at 30 frames per second. This captures a video file of particles moving under Brownian motion within a field of view of

approximately 100 μm × 80 μm × 10 μm (Fig. 2.34). NTA can find out the difference between a particle structure and a material from the difference in the dispersion intensity on the surface of a particle [1].

#### 2.3.6.2.2 Tracking in two dimensions

Within the field of view, particles are seen moving under Brownian motion, either directly by eye using the microscope oculars or via the camera. The proprietary NTA software records a video file of the particles viewed and then simultaneously identifies and tracks the centre of each particle on a frame-by-frame basis. The image analysis software then determines the average distance moved by each particle in the $x$ and $y$ directions. This value allows the particle diffusion coefficient ($Dt$) to be determined from which, if the sample temperature $T$ and solvent viscosity $\eta$ are known, then the sphere-equivalent hydrodynamic diameter d of the particles can be identified using the Stokes–Einstein equation (Eq. (2.12)) [1].

$$Dt = \frac{TK_B}{3\pi\eta d} \tag{2.12}$$

where $K_B$ is Boltzmann constant.

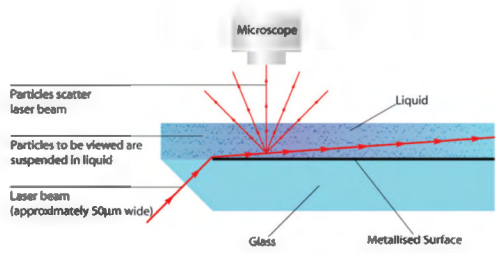


**Figure 2.34** Schematic of the optical configuration used in NTA.

#### 2.3.6.2.3 Motive forces

It is possible to apply an electric field through the sample by use of immersed electrodes. This induces electrophoresis of charged particles from which their ZP, $\zeta$, can be determined. This parameter is central to colloidal performance and stability in a wide range of nanoparticulate materials and products, a high surface charge-minimising aggregation of the dispersion because of charge repulsion. Thus, a measure of ZP determines tendency for sample aggregation over time but varies with pH, temperature, concentration and particle size.

NTA is capable of measuring directly, in real time and on a particle-by-particle basis, the electrophoretic velocity and polarity of charged nanoparticles under an applied field. However, unlike conventional high-frequency ZP analysis measuring instruments, applying a constant electric field through an aqueous liquid causes a parabolic flow profile in the sample chamber due to electro-osmosis, and it is independent of charged particle motion (Fig. 2.35). A particle's velocity observed by NTA at any point will therefore be a combination of both solvent electro-osmosis and particle electrophoresis [1].

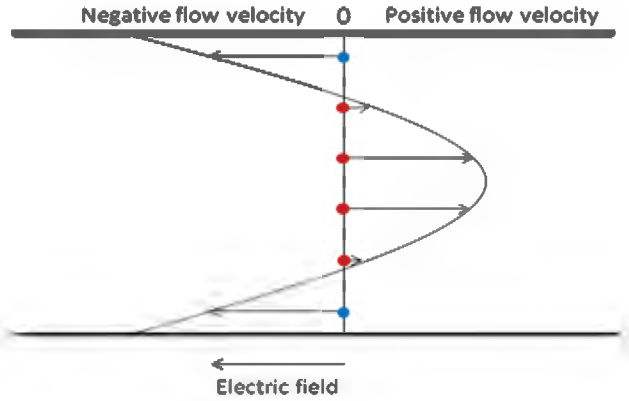


**Figure 2.35** The solvent electro-osmotic profile generated within the NTA closed system, which must be measured and subtracted from the total nanoparticle motion detected to allow the nanoparticle electrophoresis to be isolated and from which its zeta potential can then be determined.

### 2.3.6.3 Experiment and result

To measure the size and number concentration of NBs, NanoSight LM20 (NanoSight Ltd.) was used. NB solution was created by introducing $O_2$ gas into pure water with NB generator (Kyowakisetsu. Co. Ltd., BUVITAS). To measure ZP of NBs, NanoSight NS500Z (NanoSight Ltd.) was used. NB solution was produced by introducing air gas into pure water with NB generator (IDEC. Co. Ltd., NanoGALF).

NBs containing $O_2$ gas and blank sample were injected into laser module using the syringe and the light scattering observed. In NBs sample, a lot of light scattering in the view was observed. But in blank sample, nothing was observed. Analysis of NBs was carried out using "Nanoparticle Tracking Analysis (NTA)" software. In the

result, the number concentration of bubble was estimated to be 3.0E8 particles/mL, and the size and number concentration of mode peak was 72 nm and 4.6E6 particles/ml, (Figure 2.36) ZP was –53 mV. Also, the particles that have strong intensity in sample liquid could not be seen, but it was assumed that the checked light scattering were not foreign substances, such as metal powder that arose at the time of generation.

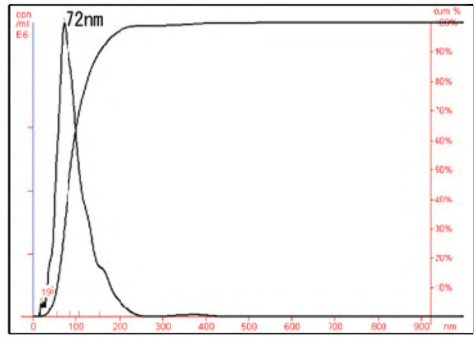


**Figure 2.36** Particle size distribution of $O_2$ NB sample. Mode size and concentration = 72 nm, 4.6E6 particles/mL. Total concentration = 3.0E8 particles/mL.

### 2.3.6.4 Conclusion

It became clear that initial studies using the NanoSight system would suggest a simple method of measuring the size and concentration of NB.

Moreover, by a ZP measurement result being added, it is assumed that it can be used for optimisation of NB generation, its physical study, etc.

## Acknowledgement

This work was supported by NanoSight Ltd., UK. NBs sample was offered by Kowakisetsu, Co., Ltd. Japan and IDEC Co., Ltd. Japan.

## References

1. Wright M, Suipa A, Sullivan J et al (2012) Nanoparticle tracking analysis (NTA) for the multiparameter analysis of nanoparticles in liquids, Part 1: Principles and Methodology.

2. M117F Application Note, NanoBubble (2009) NanoSight Ltd., UK.
3. M121 A Application Note, ZetaPotential (2011) NanoSight Ltd., UK.
4. Vasco Filipe et al (2010) Critical evaluation of nanoparticle tracking analysis (NTA) by nanosight for the measurement of nanoparticles and protein aggregates, *Pharm Res*, **27**(5), 796–810.
5. Ayako Irie (2010) The Latest Technology of Microbubbles and Nanobubbles 2. pp. 67–70 (in Japanese).

## 2.3.7 Particle Image Velocimetry System

**Masashi Yasuki**
*Seika Corporation, Tokyo 100-0005, Japan*
myasuki@jp.seika.com

### 2.3.7.1 Introduction

Particle image velocimetry (PIV) is a technique to measure velocity based on displacement of small particle within small time separation.

As PIV can be used for both gas and liquid flow, it is widely used among many R&D fields.

Originally, it was developed for aerodynamic measurements for aircrafts etc, and now it is widely used from large-scale measurements such as full-scale wind tunnel testing for automobile to microscale measurements such as microfluidic research in bio- and life science field. It has become necessary measurement system in fluid dynamics.

This paper explains the principle of PIV, recent system configuration of PIV system and its performance.

#### *2.3.7.1.1 Principle of PIV*

In PIV, small particles are seeded to the flow in advance and visualised by illuminating with so-called laser light sheet, which is generated by expanding the laser beam to planer state.

Taking two photographs with short time separation and applying cross correlation to these two images to get thousands of near instantaneous velocity vectors for whole images. From these velocity vectors, it is possible to calculate several flow parameters, such as vorticity and flow strains. Furthermore, parameters such as

turbulent intensity can be obtained by averaging the several tens and several hundreds of these instantaneous velocity fields.

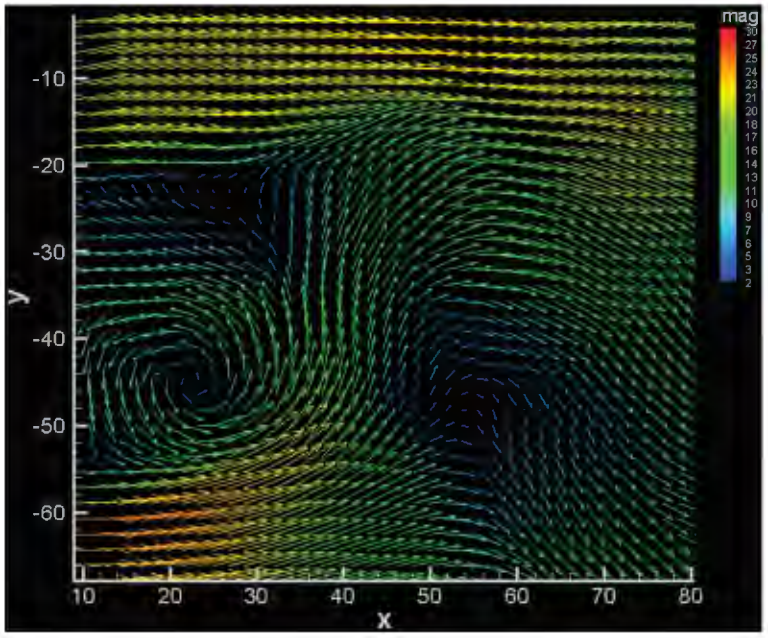


**Figure 2.37** Velocity vector map by PIV.

#### *2.3.7.1.2 Image capture by frame straddling*

In PIV, the flow is visualised by illuminating with laser light sheet, and particle image is taken by a camera placed normal to the light sheet. At this time, two images with small time separation are captured. To do this, a double pulse laser that can fire two pulses with flexible time separation and a camera that has a double shutter function are used in combination.

A double shatter camera is a digital CCD camera or digital CMOS camera, which can capture two images with very short time separation. Using it in synchronisation with a double pulse laser, it is possible to take two images with minimum time separation of down to about 70 ns (minimum time separations differ according to manufacturers and models). The actual time separation between two images is decided by the timing of firing double pulse, not by the time between two frames. This synchronised imaging is called frame straddling.

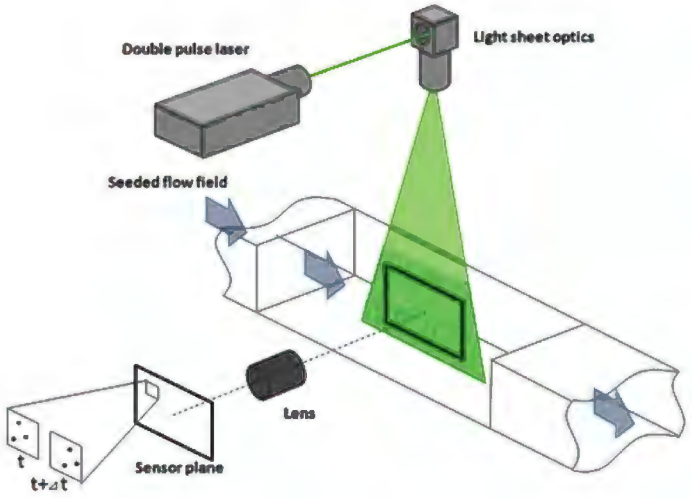


**Figure 2.38** Principle of PIV.

It is possible to apply any velocity range by setting the time separation so that the average particle displacement between two images is several pixels apart.

#### *2.3.7.1.3 Seeding*

To visualise flows, smokes or small particles are mixed to flows. This is called seeding, and particles used for seeding is called tracer particles.

For air or gas flows, small droplets of about 1 micron in size are used, and a Laskin nozzle-type seeding generator is most useful for seeding. For water or liquid flows, solid particles or microbubbles are used.

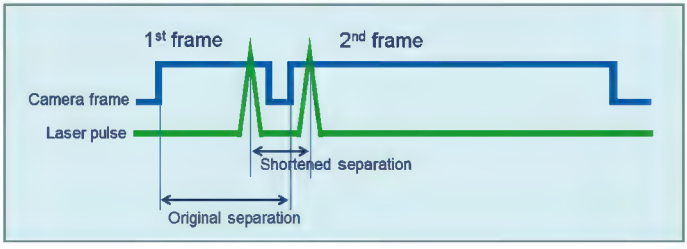


**Figure 2.39** Frame straddling.

Various material of solid particle, such as Nylon, Polystyrene and glass particles, is used depending on specific gravity of liquid.

Particle size varies depending on measurement area size, spatial resolution of camera sensors, etc.

It is useful to use microbubbles as a seeding for flow measurements with large quantity such as water tunnels. Microbubble does not require collecting and cleaning after measurements.

In such cases as spray application, seeding is not required because the measuring object itself is small particles.

However, even in the spray application, seeding is required for measuring regions outside of spray or entrainment of the spray.

In any cases, one must be careful that excessive seeding may alter the flow property.

### 2.3.7.2 PIV system

Here, a SEIKA Koncerto2D-PIV system is explained as an example of standard 2D-PIV system, which is currently most generally used.

#### *2.3.7.2.1 System configuration of 2D-PIV system*

##### *2.3.7.2.1.1 Software*

Koncerto software is integrated PIV software, which performs all processes required in PIV, such as hardware control of lasers and cameras, digital filters for image processing, pre-processing of background subtraction, etc., velocity evaluation of PIV processing, post-processing of data validation and data visualisation.

##### *2.3.7.2.1.2 Timing controller*

A timing controller Seika TT1680 has eight physical output channels, eight logical output channels and eight physical input channels. It synchronises not only PIV system itself but also a more complex synchronisation such as rotating machineries.

##### *2.3.7.2.1.3 Double pulse laser*

A double pulse laser consists of two set of independent frequency-doubled pulsed Nd:YAG lasers. Two beams are combined by polarising optics to single beam. Thus, the time separation of two pulses is completely flexible. Typical specification of each laser is as follows. Wave length is 532 nm (green), and pulse duration is 5–10 ns. Repetition rate is 10–15 Hz. Pulse energy is 10–200 mJ.

#### *2.3.7.2.1.4 PIV camera*

PIV camera is digital CCD of CMOS camera, which must be capable of frame straddling mentioned before.

Typical specification is as follows. Spatial resolution is 1–5 Megapixel. Frame rate is 5–100 frames per second. It can capture two frames with a minimum time separation of 1 ms. Time resolution of PIV is less than a half of frame rate. These specifications are depending on models.

#### *2.3.7.2.1.5 Light sheet optics*

Light sheet optics is to generate laser light sheet to illuminate flow field with required image area. Seika BZ-60 light sheet optics is adjustable sheet angle and focal length.

### *2.3.7.2.2 PIV analysis*

#### *2.3.7.2.2.1 Cross correlation analysis on Koncerto*

Koncerto employs variety of PIV analysis algorithms based on FFT cross correlation. Here, the concept of these methods is explained.

**Standard FFT cross correlation** Figure 2.40 is the process of standard FFT cross correlation. An image A in a drawing is the first image and an image B is the second image. Two-dimensional FFT is applied to the interrogation area, which is the small area typically 32 × 32 pixels in both images with same location to obtain a correlation plane. Next, a peak search is performed to correlation plane, and a correlation peak is obtained. Then, the final displacement is obtained by sub-pixel fitting.

**Double (multiple) correlation** Double (multiple) correlation is a technique to enhance a signal-to-noise ratio of cross correlation. Multiplying two correlation planes, which are obtained from two interrogation windows close to each other, to increase regular signal and decrease irregular noise. Number of windows, rate of overlap and direction (horizontal or vertical) are selectable by the software.

**Multiple pass correlation** Multiple pass correlation is a technique to increase the accuracy of correlation. It is so-called iterative method.

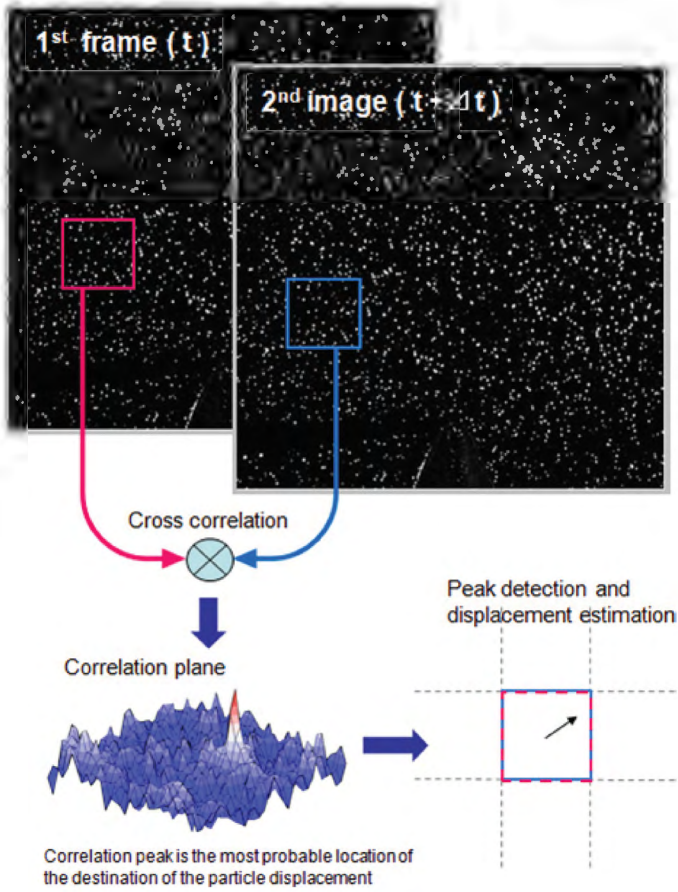


**Figure 2.40** Standard FFT correlation.

The result of standard cross correlation is used as a predictor to shift an interrogation window in a second image and apply standard cross correlation again to get higher correlation peak than previous time. Applying this procedure several times iteratively, we get accurate result. Number of iteration is selectable by the software.

**Multiple grid correlation** Multiple grid correlation is also a technique to increase the accuracy of correlation. It is so-called hierarchical method. Same as multiple pass correlation, the iterative operation is applied, in each iteration, the interrogation window are

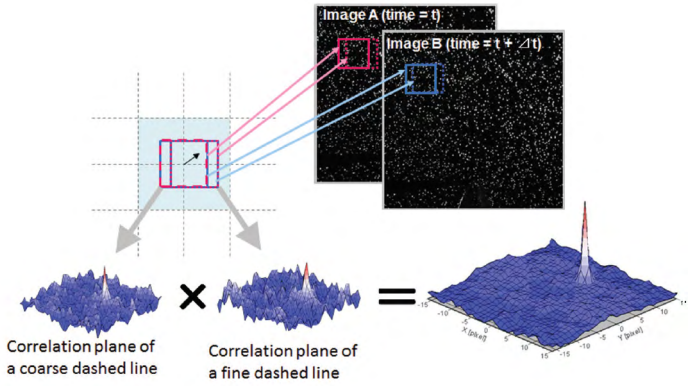


**Figure 2.41** Double (multiple) correlation.

divided by four. It has effect of extending dynamic range, increasing spatial resolution and applicable in the case of rotation in an interrogation window.

**Image deformation correlation** Window shifting by a predictor in the multiple pass correlation and the multiple grid correlation mentioned before is a shift by pixels. In the image deformation correlation, surrounding multiple predictors are used to deform images. Thus, sub-pixel image shift is possible. It is applicable if there is a deformation and/or rotation in an interrogation window, and more accurate result is obtained.

**Central difference interrogation** The iterative operations, such as multiple pass correlation, multiple grid correlation and image deformation correlation mentioned before, are explained based on forward difference interrogation for the simplicity. Central difference interrogation is a technique to apply window shifting for both images. An interrogation window in second image is shifted by half of a predictor, and an interrogation window in first image is shifted back by half of predictor. The better result can be obtained in such a measurement case that near wall and obstacles in the flow.

#### *2.3.7.2.2.2 Post-processing*

Post-processing is after processing of cross correlation analysis, and velocity vector validations, statistical processing and data display are included.

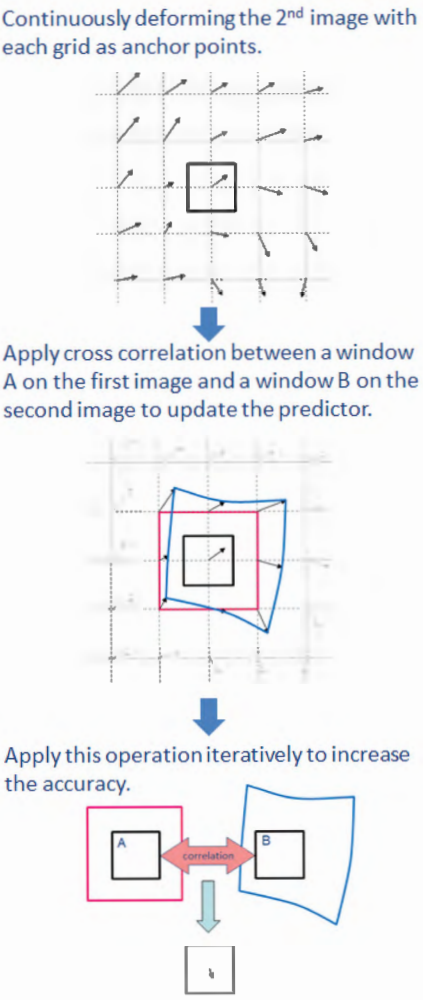


**Figure 2.42** Image deformation correlation.

**Velocity vector validations** In PIV, several thousands of velocity vectors can be obtained from an image pair. However, all these vectors are not always analysed correctly and error vectors are generated by various factors.

A vector validation first determines correct or error of a vector, remove it if it seems erroneous and apply interpolation to fill a hole.

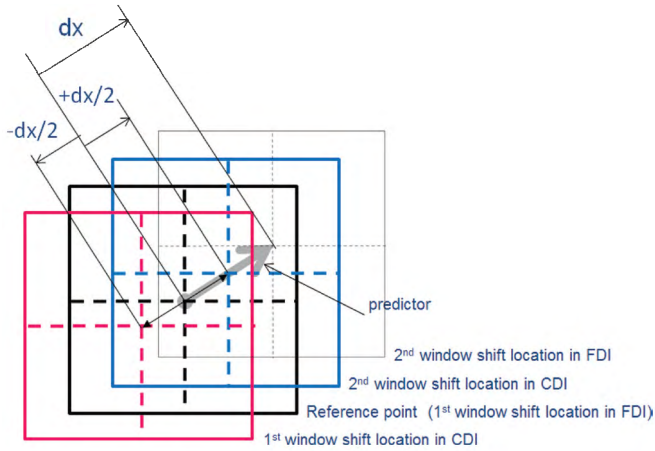


**Figure 2.43** Central difference interrogation.

There are two types of validation filters, a global filter and a local filter. Global filters are applied to all vectors such as a standard deviation filter and a max displacement filter. Local filters such as median filter and average filter are applied to local areas typically $3 \times 3$ vectors.

**Statistical processing and calculation of flow parameters** Average vector field and Root mean square (RMS) vector field can be calculated as statistics. Calculation of flow parameters such as vorticity and turbulent intensity is possible.

**Statistical processing and calculation of flow parameters** Average vector field and Root mean square (RMS) vector field can be calculated as statistics. Calculation of flow parameters such as vorticity and turbulent intensity is possible.

**Automated operation** Batch processing and script processing are possible as an automated operation to apply various PIV processing to multiple images.

**Various PIV systems** Lastly, other PIV systems are introduced. A stereo PIV system can measure three velocity components in two-dimensional plane. A time-resolved PIV system is a very high time resolution (up to about 40 kHz) PIV system, which employs a high-speed video camera and a high-repetition rate pulse laser. Micro-PIV

can measure microscale velocity field such as microfluidic ships using optical microscope. Volume PIV system is developed to measure three component measurements in a three-dimensional cube. These systems can be combined to integrate complex PIV systems.

## References

1. Raffel M, Willert C, Kompenhans J (1998) *Particle Image Velocimetry, A Practical Guide*, Springer, Berlin.
2. The Visualization Society of Japan (2002) PIV hand book, Morikita Publishing Co., Ltd.